ADVANCED MATERIALS
www.advmat.de

Accelerated Development of Colloidal Nanomaterials Enabled by Modular Microfluidic Reactors: Toward Autonomous Robotic Experimentation

*Amanda A. Volk, Robert W. Epps, and Milad Abolhasani**

In recent years, microfluidic technologies have emerged as a powerful approach for the advanced synthesis and rapid optimization of various solution-processed nanomaterials, including semiconductor quantum dots and nanoplatelets, and metal plasmonic and reticular framework nanoparticles. These fluidic systems offer access to previously unattainable measurements and synthesis conditions at unparalleled efficiencies and sampling rates. Despite these advantages, microfluidic systems have yet to be extensively adopted by the colloidal nanomaterial community. To help bridge the gap, this progress report details the basic principles of microfluidic reactor design and performance, as well as the current state of online diagnostics and autonomous robotic experimentation strategies, toward the size, shape, and composition-controlled synthesis of various colloidal nanomaterials. By discussing the application of fluidic platforms in recent high-priority colloidal nanomaterial studies and their potential for integration with rapidly emerging artificial intelligence-based decision-making strategies, this report seeks to encourage interdisciplinary collaborations between microfluidic reactor engineers and colloidal nanomaterial chemists. Full convergence of these two research efforts offers significantly expedited and enhanced nanomaterial discovery, optimization, and manufacturing.

1. Introduction

Solution-processed organic,[1–3] metallic,[4–6] and semiconductor[7,8] nanomaterials, possess unique size-related physicochemical, optical, magnetic, and electronic properties. These materials have enabled groundbreaking advancements in a variety of applications including catalysis,[9–11] drug delivery,[12,13] data storage,[14] and solar cells.[15] Different nucleation and growth models such as LaMer burst nucleation,[16] Ostwald ripening,[17] Finke–Watzky two-step mechanism,[18] orientated attachment,[19] and coalescence[20] have attempted to explain the mechanisms through which nanoparticles are formed in solution. Although it is generally accepted that solution-phase synthesis of colloidal nanoparticles follows a nucleation and growth mechanism, the key parameters controlling nanoparticle size, size distribution, morphology, and properties are still not well-understood. Prior studies suggest that the degree of supersaturation, surface energy, reaction temperature, and reaction time significantly impact the nanoparticle nucleation and growth kinetics.[7,8,21–23] However, the flask reactors most often implemented in colloidal nanomaterial synthesis studies—are unable to alter the rate of these effects to the extent necessary for systematic control. The development of most solution-processed nanomaterial syntheses is, therefore, hindered by the limitations of the techniques utilized to synthesize and characterize them.

Microfluidic reactors, due to their inherently fast mass and heat transfer rates and material consumption superiority over batch reactors, have become a burgeoning frontier for advanced colloidal nanomaterial synthesis. Nevertheless, compared to other fields such as genomics,[24] organic synthesis,[25] and biomedicine,[26,27] the use of microfluidic reactors for colloidal nanomaterial synthesis is in a relative infancy. This disparity may be attributed to previous limitations of microfluidic reactors, such as the complex microfabrication of fluidic devices[28–32] amenable to inorganic synthesis reactions. However, over the past five years a growing number of readily accessible, reconfigurable, and application-ready fluidic technologies, such as tube-based flow reactors, have successfully been demonstrated for the controlled synthesis of high-quality colloidal semiconductor nanocrystals[33–35] and various other nanomaterials.[36,37] Considering the growing availability of low-cost and highly versatile modular microfluidic reactors, colloidal nanomaterial synthesis is approaching a paradigm shift toward flow synthesis for accelerated fundamental and applied studies and the sophisticated synthesis of next-generation advanced functional nanomaterials.

Most colloidal nanomaterials exhibit structure,[10,38] size,[39–41] and composition-dependent[42] properties which dictate their application and downstream performance characteristics. These effects have been widely documented and summarized in a collection of existing review articles,[43,44] and separate

A. A. Volk, R. W. Epps, Prof. M. Abolhasani
Department of Chemical and Biomolecular Engineering
North Carolina State University
911 Partners Way, Raleigh, NC 27695, USA
E-mail: abolhasani@ncsu.edu

The ORCID identification number(s) for the author(s) of this article can be found under https://doi.org/10.1002/adma.202004495.

DOI: 10.1002/adma.202004495

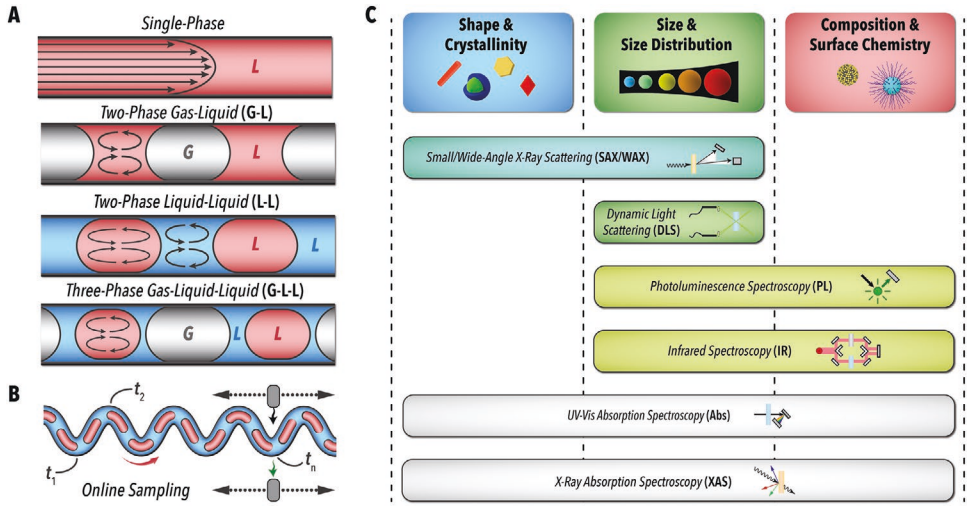

Figure 1. A) Illustration of single-phase (continuous) and various multiphase flow regimes which may be used for controlled synthesis of colloidal nanomaterials. G: Gas, L: Liquid. B) Illustration representing online sampling techniques which can be performed at a fix point or moved along a reactor length, corresponding to different residence (reaction) times (t_n). C) Overview of the currently available online nanomaterial characterization techniques integrated with microfluid reactors, organized by the colloidal nanomaterial properties they have been used to monitor.

publications have effectively summarized the basic principles governing microfluidic devices.[45–48]

This progress report presents an overview of recent research efforts focused on controlled and accelerated flow synthesis of colloidal nanomaterials. We provide a foundational framework necessary for the facile adoption of flow-based colloidal synthesis strategies toward accelerated synthesis, online monitoring, and controlling (i) size, (ii) shape and structure, and (iii) composition of nanomaterials across a broad range of colloidal nanomaterial syntheses (**Figure 1**). In addition, we discuss recent developments in utilization of microfluidic reactors for colloidal nanomaterial synthesis automation and optimization and their implications in future accelerated nanomaterial development studies by converging with rapidly emerging artificial intelligence (AI)-based decision-making strategies. Finally, we discuss the current opportunities and prospects of flow technologies in alleviating labor-and material-intensive experimentation for process–structure–property mapping of advanced functional nanomaterials.

2. Colloidal Nanomaterial Synthesis: Batch versus Flow

Advantages of microfluidic reactors can be understood by comparing the physics of their characteristic mass/heat transport length scale to their macroscale analogs.[49] Specifically, at micro/millifluidic characteristic length scales, the following surface effects dominate over volumetric effects: First, in microreactors, viscous forces dominate over inertial forces, and flow exists in a laminar regime (i.e., Reynolds number, Re < 2000). Fluidic mixing in the laminar flow regime is primarily by molecular diffusion, which simplifies analysis and control of molecular transport.[50] Second, interfacial tension and capillary forces dominate over gravitational forces. This phenomenon has been exploited in microfluidics for the fabrication of microscale separation systems[51] as well as droplet generation.[52–54] Finally, the significantly higher surface-to-volume ratio of micro/millifluidic reactors compared to macroscale reactors results in superior mass and heat-transfer rates (process intensification). Enhanced transport rates reduce the spatiotemporal variability of reactor conditions, and therefore allow for an ideal reaction environment for nanomaterial syntheses with exceptional control and reproducibility. In addition, enhanced transport rates increase reaction rates and thereby increase the time and material efficiency of microfluidic systems. Since low active (i.e., heated and pressurized) reactor volumes (<1 mL) may be achieved without sacrificing overall colloidal synthesis throughput, microfluidic reactors are viable "safer by design" options for the controlled synthesis, optimization, and end-to-end manufacturing of colloidal nanostructures which require hazardous reactants.

2.1. Single and Multiphase Flow Nanomaterial Synthesis

The most conventional configuration of microfluidic reactors is single-phase flow synthesis (Figure 1A), which is operated under a laminar flow regime, thereby resulting in a highly predictable and well-controlled flow format. An additional benefit of single-phase flow reactors is that reagents downstream can be easily added for multistep nanomaterial synthesis. However, single-phase microfluidic synthesis strategies suffer from specific drawbacks that can limit their application in the synthesis of high-quality nanomaterials. Due to their parabolic velocity profile, laminar flow reactors have nonuniform residence time distributions that may result in variegated nanomaterial properties for a given flow synthesis condition. An effective approach to the concentration and velocity variations encountered in single-phase flow is multiphase segmented flow (droplet or slug flow), depicted in Figure 1A. Depending on interfacial forces, viscous forces, and inertial forces, other multiphase

flow formats may be formed apart from segmented flow, such as stratified[55] and core-annular flow.[56] However, because of their demonstrated benefits in controlled colloidal nanomaterials synthesis, in this report, we focus on the application of segmented flow synthesis strategies.

Two-phase flow microreactors are among the most extensively studied flow systems and may be classified as (immiscible) liquid-liquid (L-L) or gas-liquid (G-L) flow formats.[57] For the case of L-L two-phase flow, the continuous phase is the phase that preferentially wets the microreactor wall. In G-L systems, liquid slugs are separated by discrete gas phases. In L-L and G-L segmented flow systems, recirculating flow patterns inside droplets or slugs (Figure 1A) is caused by the shear force from the continuous phase or microreactor channel, respectively.[58–60] This recirculating flow enhances mixing by reducing the effective diffusion pathlength within dispersed phase (i.e., slugs or droplets), leading to a more homogeneous reaction environment and resulting nanomaterial properties. With two-phase flow systems, both phases may also serve as reactants. In this case, the fast mass transport facilitated by internal flow circulations can enhance the reaction rates beyond the capacity of batch systems. As we will detail in this report, interfacial mass transport dynamics in immiscible reactive systems may be exploited to obtain precise nanomaterial properties.

Beyond enhanced efficiency, microfluidic platforms present their greatest advantage in the facile ability to access and decouple large reaction parameter spaces, i.e., through the precise control of residence (reaction) time, rate of mixing, and precursor composition and concentration. Noninvasive, online nanomaterial characterization techniques may be used to characterize such high-dimension parameter spaces and provide information at reaction times on the order of milliseconds.[48] Residence (reaction) time studies may be performed using online characterization techniques by changing the total flow rate and maintaining the sampling point constant, or by changing the sampling point along the length of the reactor (Figure 1B).[61] Online monitoring capabilities which have been used to monitor size, shape, and composition of colloidal nanomaterials in flow are summarized in Figure 1C. X-ray scattering, photoluminescence (PL) spectroscopy, UV–vis absorption (Abs) spectroscopy, and X-ray absorption spectroscopy (XAS) have been used for online characterization of colloidal nanomaterials synthesized in flow and will be discussed in more detail. Dynamic light scattering (DLS) and infrared spectroscopy (IR), although both have successfully been integrated with microfluidic reactors, have not been applied as extensively due to several limitations.[62,63] For DLS-based nanomaterial size measurements on pressure-driven flow, relatively low shear rates are required which are difficult to predict due to complex dependencies on experimental setups.[62] Transmission IR techniques require transparent sampling ports in the microreactor and can suffer from signal-to-noise issues from absorbing fluids. Another IR approach, attenuated total reflection (ATR) IR, can only sample near the ATR crystal surface which can become contaminated due to fouling.[63] Despite these challenges, advancements in micro/millifluidic reactor designs and IR absorption enhancement techniques make DLS and IR characterization promising tools for online monitoring of fluidic colloidal nanomaterial syntheses.[64] In addition to Abs and PL spectroscopy, the relatively low acquisition times of DLS and IR characterization techniques make them promising online nanomaterial characterization techniques for autonomous nanomaterial synthesis and optimization.

The integration of device automation strategies has been shown to extend the capacity of microfluidic platforms to high-throughput user-assisted experimentation. Furthermore, fully automated microfluidic synthesis reactors have been integrated with data science and AI-based decision-making algorithms to achieve self-optimizing nanomaterial synthesis platforms.[65] Employing such self-driven colloidal nanomaterial synthesis reactors, high-quality nanomaterials has been successfully synthesized through the rapid, unattended optimization of colloidal synthesis parameters.[65] Microfluidic reactors, therefore, have the means to control, isolate, and optimize synthesis properties for different classes of colloidal nanomaterials (e.g., semiconductor nanocrystals, metal, and metal oxides) with efficiency, control, and uniformity unattainable through batch systems.

2.2. Microreactor Design for Controlled Nanomaterial Synthesis

The two dominate microreactor designs used for micro/millifluidic synthesis of colloidal nanomaterials are microfabricated and tube-based microreactors. When selecting which microreactor to use, primary considerations should be application, chemical compatibility, temperature and pressure resistance, and the balance between the intricacy of microreactor design and fabrication. Microfabricated microreactors, compared to their tubular counterparts, have a high capacity for specialization.[66–68] Advanced microchannel configurations, online monitoring capability, small microreactor footprints, and low system volumes are among the traits that contribute to their diverse functionalities. Polydimethylsiloxane (PDMS) microreactors can be made with complex microchannel geometries via photolithography, soft lithography, and print-and-peel methods.[69] However, PDMS has limited mechanical strength and chemical compatibility. In addition, PDMS has poor thermal conductivity, making heated PDMS microreactors susceptible to hotspots. Improved thermal conductivity and chemical compatibility can be obtained with silicon-based microreactors, which are often used with a transparent substrate (e.g., glass) for optical access.

Enabled by reactive etching (wet or dry), advanced microchannel configurations in silicon-pyrex microreactors have been developed to separate temperature zones in a single microreactor which can accommodate 1.5 m of microchannel length in a footprint with dimensions on the order of centimeters (**Figure 2**A).[70] Recently, transparent glass microreactors with advanced microchannel configurations for optimized heat and mass transfer have also been introduced commercially and used in production scale photochemical reactions. Corning's Advanced-Flow G3 photoreactor, depicted in Figure 2B, has recently been utilized for the photochemical synthesis of Au nanoparticles at production scale (≈360 L of aqueous Au nanoparticles a day), providing an alternative to high-temperature reduction reactions.[71,72]

Despite the advantages of microfabricated reactors, advanced high-resolution fabrication techniques can pose a notable

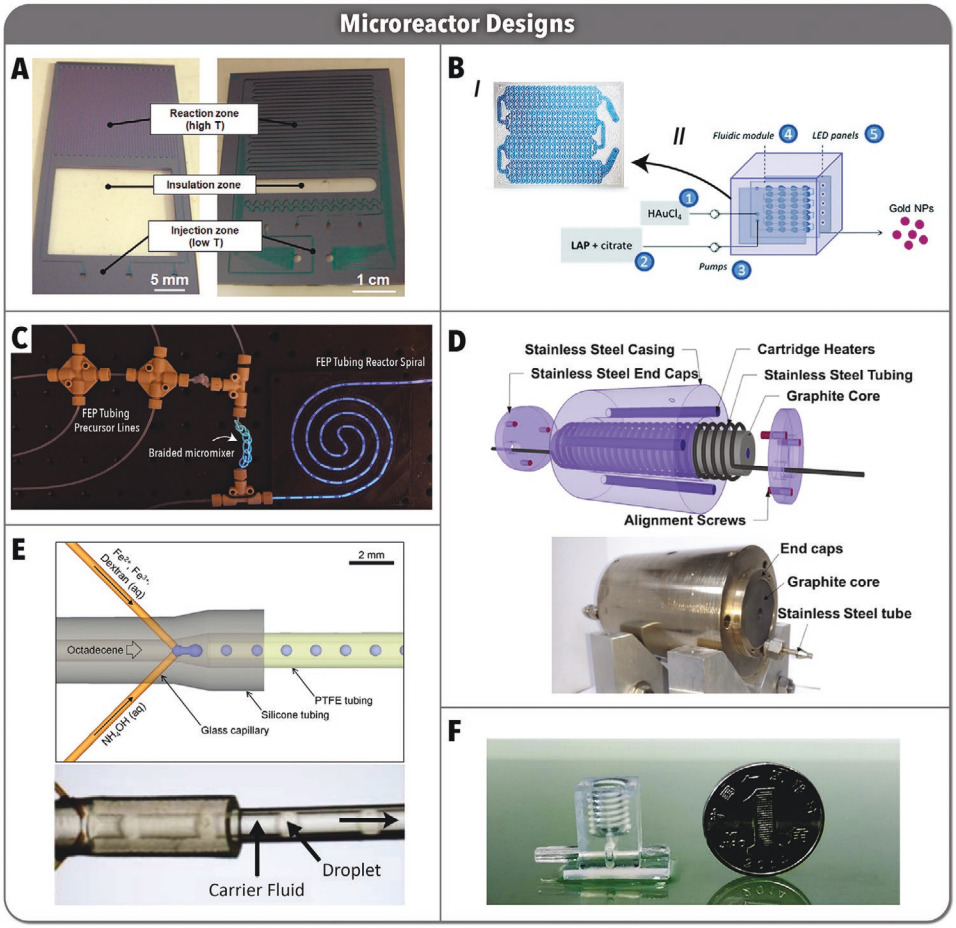

Figure 2. A) Photographs of silicon-pyrex microfabricated reactor with an insulating etched Si gap, from Marre et al., designed for high-temperature/pressure reactions. Adapted with permission.[70] Copyright 2010, American Chemical Society. B) (I) Corning Advanced-Flow G3 microfabricated glass flow reactor module, detailed by Bianchi et al., and (II) schematic of the photoreactor flow synthesis platform for the production scale synthesis of Au nanoparticles. Adapted with permission.[71] Copyright 2020, Royal Society of Chemistry. C) FEP tube-based flow reactor incorporating an FEP tube braided (static) micromixer and commercially available fluidic junctions, from Epps et al. Adapted with permission.[65] Copyright 2020, Wiley-VCH. D) High-temperature stainless steel tubing and shell reactor, from Kumar et al. Adapted with permission.[34] Copyright 2017, Wiley-VCH. E) Glass capillary and polytetrafluoroethylene (PTFE) droplet reactor, from Kumar et al. Adapted with Permission.[74] Copyright 2012, Royal Society of Chemistry. F) 3D-printed microreactor detailed in Li et al. Adapted with permission.[76] Copyright 2019, Royal Society of Chemistry.

barrier to inexperienced users as they often entail precise etching, thermoforming, or channel casting. In addition, current chip-based designs inhibit reconfiguration, making reactor prototyping and design exploration labor and cost-intensive endeavors. In response to these limitations, tube-based and plug-and-play flow systems have recently risen in popularity as facile, low-cost alternatives for controlled synthesis of colloidal nanomaterials.[61,73]

Tube-based flow reactors capitalize on commercially available fluoropolymer and metal tubing (Figure 2C,D, respectively) in combination with both custom and off-the-shell fluidic junctions and accessories.[34,65] In addition, glass capillaries can be used in conjunction with polymer tubing for droplet formation via flow focusing, as shown in Figure 2E.[74] These systems may be assembled and repaired at a rate unattainable in microfabricated reactors and are compatible with a wide range of solvents without the need for additional surface modification (such as the formation of an oxide layer on patterned silicon microreactors). While tubular reactors are behind in certain capacities compared to microfabricated reactors, there is a growing collection of modular components for tube-based colloidal syntheses, with applications ranging from online spectral monitoring to passive micromixing.[75]

Similar to capillary tubing, additive manufacturing strategies which may be used for microreactor fabrication have become commercially available and cost-effective. Additive manufacturing techniques can provide the small footprints and advanced microchannel configurations of lithography-based microfabrication strategies with less complicated fabrication steps. For example, a 3D-printed microreactor with a 1.5 mm microchannel diameter was recently manufactured using a desktop 3D printer with 0.05 mm layer resolution for the continuous flow synthesis of organometal halide perovskite nanocrystals (Figure 2F).[76] In addition to microreactor channels, functional microfluidic components, ranging from passive micromixers to pumps, can also be created through

3D-printing. Furthermore, modular and reconfigurable microfluidic systems have been demonstrated using 3D-printed microchannel components.[77–79] Regardless of the microreactor design, microscale fluidic platforms provide an adaptable, modular, and reconfigurable approach to reactor construction which can meet the physical/chemical demands of most nanomaterial syntheses.

3. In-Flow Size and Size Distribution Control of Colloidal Nanomaterials

Across the field of colloidal nanoscience, size plays a critical role in the properties (e.g., physicochemical, optoelectronic) of most nanomaterials. For example, within the extrinsic and intrinsic size effect regimes of noble metal nanoparticles, particle dimensions strongly affect surface plasmon resonance peak energy and linewidth.[80,81] Similar to the intrinsic regime of metal nanoparticles, colloidal semiconductor materials with reduced size (on the order of the exciton Bohr radius) possess size-dependent optoelectronic properties due to quantum confinement effects. Nanocrystal size also affects mechanical and catalytic properties, such as shape memory behavior and turnover frequency of metal–organic framework (MOF) and metal-alloy nanocrystals, respectively.[82,83] Because of the strong influence of size on nanomaterial properties, attaining highly monodisperse nanoparticle populations (i.e., minimum size polydispersity) is one of the key goals in the development of colloidal synthetic routes. Despite this requisite, most colloidal nanoscience research driven by flask-based synthesis techniques fail to control synthesis conditions to the extent necessary to produce replicable and narrow nanomaterial size distributions. Variability in experimentalists, equipment, and heat and mass transfer rates pose an obstacle to consistent colloidal synthesis results, specifically in colloidal syntheses with fast formation kinetics.

A limited understanding of early reaction time scales and restricted control of nucleation and growth mechanisms—i.e., monomer formation, diffusion to growth surface, reaction rate, ligand stabilization—may lead to large nanomaterial size distributions. In response to these limitations, recent efforts have leveraged the enhanced transport rates and reaction control offered by flow processes to synthesize size-tuned, monodisperse nanomaterials. These studies have utilized a wide range of online characterization methods developed for real-time monitoring nanomaterial size and polydispersity in microreactors. UV–vis absorption and PL spectroscopy are among the more common noninvasive online characterization techniques for optically active colloidal nanomaterials and may be conducted using commercially available optical flow cells. Utilizing either absorption or PL spectroscopy, combined with the correct correlations or mass approximation models for a given nanomaterial, the modal nanoparticle size and polydispersity may be extracted from online-obtained optical spectra.[84,85] More recently, alternative techniques such as XAS have been integrated with microfluidic reactors. Coordination number and interatomic distances obtained by XAS may be used to obtain small (<5 nm) particle sizes for various structures through a number of methods, such as estimating particle diameter based off of the mean coordination number of outer shell atoms or by the reduction of metal–metal coordination numbers relative to the bulk.[86] Furthermore, photothermal spectroscopy techniques, such as differential detection photothermal interferometry (DDPI), have been used in flow to determine plasmonic nanoparticle size distributions from electrostatic approximations and Mie theory calculations.[87]

3.1. Multistage Microfluidic Reactors

Multistage microfluidic reactors with rapid heating and cooling rates have been demonstrated to be an effective tool for the controlled synthesis of a wide range of colloidal nanomaterials (e.g., semiconductor quantum dots (QDs), noble metal nanoparticles) by either separating heating/cooling zones, the nucleation and growth stages, or by enabling continuous addition of chemical precursors during the microfluidic synthesis. Kumar et al. utilized a temperature-controlled stainless-steel flow reactor, for the controlled synthesis of cadmium selenide (CdSe) anisotropic nanoparticles and zinc selenide (ZnSe) nanorods.[34] The heating rate of the stainless-steel flow reactor (through heat transfer simulation) was reported to be 245 °C s^{-1}, a rate which significantly surpasses the capabilities of analogous flask systems. The heated stainless-steel flow reactor was immediately followed by a microchannel cooling section, which was designed to rapidly quench the synthesized nanoparticles to control the size and polydispersity of the in-flow synthesized nanomaterials. The precise control over reaction temperature and residence time was used to rapidly determine the optimal parameters for nanorod ripening and produce nanorods with a width variance of 16%, improving upon the 30% variance of batch syntheses.

Other multistage microfluidic reactor designs have used sequential reagent injections into moving reactive phases for size-controlled, multistep colloidal nanomaterial syntheses. In droplet-based multistep flow syntheses, reagents can be incorporated downstream either by droplet fusion[88] or direct injection into a preformed droplet.[89] In L-L droplet microfluidic reactors, employing droplet fusion and direct injection requires complex microreactor designs and strict flow stability, both drawbacks to facile multistep synthesis. These drawbacks have been overcome by the introduction of a three-phase (liquid-liquid-gas) flow format.[90] In the three-phase flow synthesis platform presented by Nightingale et al., reactive phase reagents were continuously flown via a T-junction into a three-phase segmented stream consisting of a carrier phase, droplet phase, and gas phase.[90] Within this type of flow regime, when the carrier fluid volume is too small to accommodate new droplet formation, it is energetically favorable for the injected droplet phase to add to the preexisting droplet rather than increase the interfacial surface area by breaking up a gas slug.[89,90] Therefore, the use of a gas phase not only created uniformly spaced droplets but also suppressed the formation of new droplets and improved droplet-flow stability. These advantages were confirmed by calorimetric analysis of two-phase versus three-phase reagent additions. Calorimetric analysis was also used to determine the stable flow rate range of the droplet addition streams, demonstrating a simple high-throughput method to screen flow synthesis parameter effects on droplet size and reagent mixing. Viability of the multistage injection strategy toward multistep

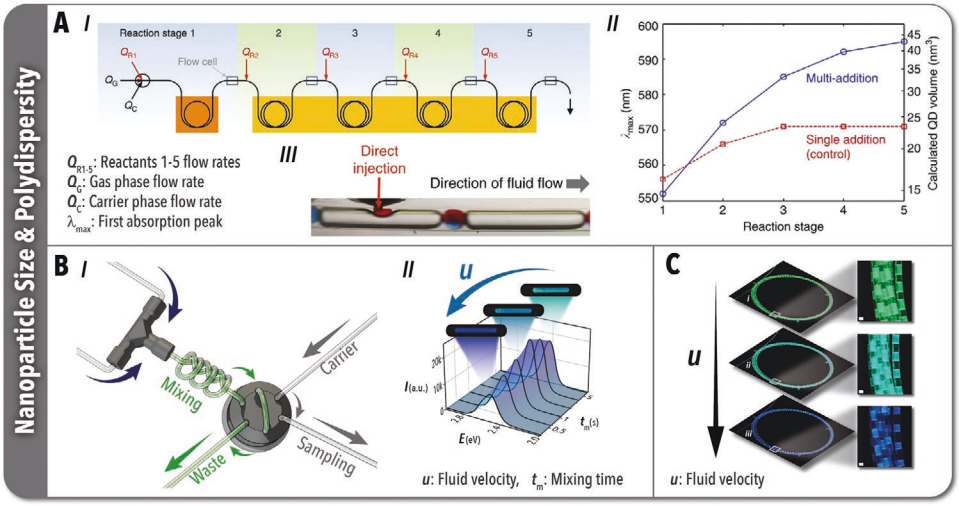

Figure 3. A) (I) Schematic of a five-stage microfluidic reactor utilizing a three-phase flow format developed by Nightingale et al. (II) PL peak emission of CdSe QDs synthesized in flow using a multistage microfluidic reactor compared to single-stage microreactor. (III) Photograph of direct injection and three-phase flow. Adapted under the terms of a Creative Commons Attribution 3.0 International License.[90] Copyright 2014, Macmillan Publishers Limited. B) (I) Schematic of an automated microfluidic platform presented by Epps et al. used to decouple precursor mixing times from total residence times in the synthesis of $CsPbBr_3$ perovskite nanocrystals. (II) Online PL spectroscopy showed a dependence of nanocrystal size as a function of precursor mixing time. Adapted with permission.[75] Copyright 2020, The Royal Society of Chemistry. C) UV-illuminated FEP flow reactor used in the gas-liquid segmented flow synthesis of $CsPbBr_3$ perovskite nanocrystals at three different flow velocities, from Epps et al. Adapted with permission.[61] Copyright 2017, The Royal Society of Chemistry.

colloidal syntheses was demonstrated through the multistep colloidal synthesis of CdSe QDs. The developed microfluidic reactor consisted of an initial heating stage to initiate nucleation (233 °C) followed by four heating stages to promote continuous growth after additional reagent injections (200 °C), as shown in **Figure 3**AI. By incorporating flow cells with online PL spectroscopy after each microreactor stage, the growth of CdSe QDs was compared between single-stage and multistage injections for the same total available reagents (Figure 3AII). In the multistage system, larger CdSe QDs were able to be formed because of a lower number of initially nucleated particles. As a result, the multistage microfluidic synthesis platform attained a range of tunable peak emission wavelengths 30 nm larger than single-injection microfluidic reactor.

3.2. Precursor Mixing Rate

While rapid precursor mixing rate is required when aiming to produce monodisperse nanomaterials, in ultrafast colloidal syntheses, tunable advection rate variations may be utilized to control nanomaterial size, and thereby their resulting size-dependent properties, on-demand. In recent work by Epps et al.,[75] the room-temperature, ligand-assisted reprecipitation of cesium lead bromide ($CsPbBr_3$) perovskite QDs was studied in a flow reactor capable of tuning precursor mixing rates as shown in Figure 3B. Since nucleation and growth stages occur at the same temperature in a room-temperature synthesis, high mixing rates are also necessary to combat inhomogeneous reactant concentrations and polydispersity. A static micromixer, comprised solely of off-the-shelf fluoropolymer tubing in a braided configuration, was used to attain tunable precursor mixing times spanning 0.053 to 7.3 s by varying the total average fluid velocity moving through the microchannel. In a braided tubing micromixer and other geometry-driven fluidic mixing strategies, the miscible fluids are combined at a faster rate than a straight microchannel due to the asymmetric variations in fluid momentum that produce chaotic motion.[91] The developed passive micromixer was integrated into a material-efficient sampling microfluidic reactor, which enabled independent control over the mixing and colloidal synthesis times.[66] Utilizing the developed microscale flow synthesis platform, mixing-controlled emission tunability of $CsPbBr_3$ QDs spanning blue to green (2.4–2.6 eV) was demonstrated by solely varying fluid mixing rate. Shown in Figure 3C, similar results were obtained in a continuous flow system by simply varying the velocity in gas-liquid segmented flow.[61] Online UV–vis absorption and PL spectroscopy, among other nanocrystal population characterizations, were utilized to rapidly measure the peak emission energy and full-width at half-maximum of the in-flow synthesized inorganic metal halide perovskite QDs. Further application of such tunable advection rate strategies in studies of colloidal nanomaterials with fast formation kinetics could unlock both greater control and deeper understanding of mixing-controlled colloidal syntheses.

4. In-Flow Shape Control of Colloidal Nanomaterials

Similar to size, the shape of many nanomaterials influences their optical and catalytic properties. For example, the dipolar plasmon energy of gold (Au) nanoparticles will change with the degree of shape isotropy, even for comparable plasmon lengths.[92] Likewise, platinum (Pt) group nanocrystals with identical chemical compositions will have widely different

catalytic performances based on their morphology.[93] High index facet Pt structures, because of their availability of low coordination number sites, can outperform lower-index morphology counterparts by up to an order or magnitude.[94]

Although the importance of colloidal nanomaterial geometry was first recognized nearly three decades ago,[95] the application of high performance anisotropic colloidal nanomaterials, such as high-index faceted nanocrystals, has been hindered by the limitations of flask-based reactions. That is, a lack of kinetic control in batch colloidal synthesis protocols often results in low-quality seeds and nanocrystals.[96] In addition, due to the fast reaction kinetics and high index parameter space of colloidal nanocrystal growth, there is a need for greater mechanistic insight on controlling nanocrystal morphology. As a result, comprehensive studies relating colloidal synthesis parameters to structure evolution and optical properties have been elusive. Microfluidic colloidal synthesis routes have emerged as an effective way to systematically decouple several key parameters in the anisotropic growth patterns of colloidal inorganic nanomaterials. These parameters may be categorized as the following: i) kinetic factors, including rate of reactant diffusion and rate of reaction at the growth surface, which are both a function of precursor concentration, temperature, accessibility of the growth surface, and mixing; ii) thermodynamic factors, such as the surface free energy of crystal facets, which may be changed with the addition of capping agents and adsorbates.

4.1. Single-Phase Flow

Precise control of synthesis parameters is especially important in colloidal nanomaterials which are formed through nonclassical nucleation routes intermediated by nonmolecular clusters.[97,98] For example, monodisperse colloidal indium phosphide (InP) QDs grown through nonclassical nucleation pathways require multiple stages to control the dissolution or coalescence of active nonmolecular species and subsequent nanocrystal ripening and growth. Furthermore, synthesizing InP core–shell heterostructures, as well as other core–shell nanomaterials, often requires the sequential addition of shell precursors to suppress secondary nucleation.[99] Because of these complex nucleation and growth pathways, the reliable colloidal synthesis of InP quantum heterostructures and their applications in next-generation optoelectronic devices requires the realization of precise multistep syntheses. Recently, microfluidic reactors incorporating discrete reactor stages to control the primary steps of nonclassical growth have been demonstrated. Baek et al. introduced a high-pressure/temperature, single-phase microfluidic platform comprised of microfabricated silicon/pyrex modules for controlled mixing, ageing, and growth stages of InP QDs, shown in **Figure 4**A panel I. Single-phase flow allowed for the facile incorporation of six injections ports that sequentially introduced InP precursors in the InP growth stage. This multistage microfluidic reactor was then expanded to include shell growth stages for the continuous synthesis of colloidal InP/CdS, InP/ZnS, InP/ZnSe, and core–shell QDs.[67] In the shell growth microreactor modules, the shell precursor stream was divided among ten subchannels to decrease shell precursor concentrations, thereby suppressing secondary nucleation of CdS, ZnS, and ZnSe without reducing the synthesis throughput. In addition to sequential reactant addition, synthesis control was enhanced by changing the temperature profiles of each microfluidic reactor stage. Through the combined control of sequential growth stages as well as enhanced mixing and precursor diffusion under supercritical solvent conditions, InP/ZnS core/shell QDs with photoluminescence quantum yields of 35% were achieved. Online PL and absorption measurements were also used to characterize the optical properties of InP/ZnS and InP/CdS QDs with varying core sizes and shell thicknesses, respectively, demonstrating the potential of multistage microfluidic platforms and online measurements toward rapid colloidal synthesis parameter screening for high-performance core–shell heterostructures (Figure 4AII,III).

Coupled with automated flow systems, rapid online shape and size evaluation can also be utilized for the automated parameter space mapping and exploration of colloidal nanomaterials. Recently, Pinho and Torrente-Murciano introduced a

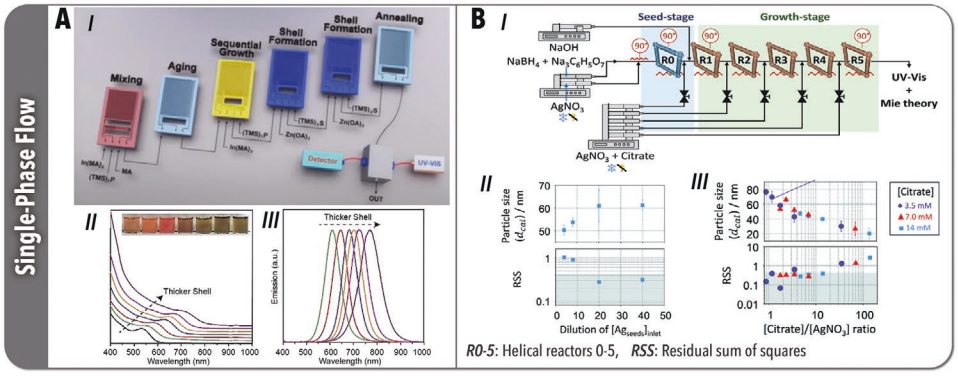

Figure 4. A) (I) Multistage, single-phase microfluidic platform developed by Baek et al. for the multistep colloidal synthesis of InP/ZnS QDs. (II) UV–vis and (III) PL spectra of the in-flow synthesized InP/ZnS core/shell QDs for varying shell thicknesses. Adapted with permission.[67] Copyright 2018, Wiley-VCH. B) (I) Schematic of the multistep, single-phase microfluidic platform for controlled in-flow synthesis of Ag nanoparticles developed by Pinho and Torrente-Murciano. UV–vis spectroscopy coupled with Mie theory-based correlations were utilized for particle size and isotropy monitoring as a function of (II) seed dilution and (III) citrate to silver nitrate ratio. Adapted with permission.[100] Copyright 2020, The Royal Society of Chemistry.

multistage flow reactor for rapid online size and shape evaluation of silver (Ag) nanoparticles via UV–vis absorption data combined with the Mie model solution of Maxwell's equations.[100] Specifically, by using a residual sum of squares (RSS) equation based on experimental and calculated optical data, the "spherical degree" of in-flow synthesized Ag nanoparticles could be evaluated. The developed multistage continuous flow reactor, shown in Figure 4B panel I, consisted of a seed stage followed by five growth stages. The seed and growth stages can be distinguished by their respective use of a strong reducing agent (sodium borohydride, $NaBH_4$) and mild reducing agent (citrate). Utilizing the developed multistage microfluidic synthesis platform, the effect of seed to growth solution ratios, number of growth stages, pH, and citrate/silver nitrate ($Ag(NO_3)$) ratio on the size, size distribution, and sphericity of Ag nanoparticles were systematically investigated. From these microfluidic studies, both a high citrate/$Ag(NO)_3$ concentration ratio as well as a high Ag seed/growth solution ratio were found to contribute to anisotropic growth of Ag nanoparticles (Figure 4BII,III). Remarkably, the multistage microfluidic synthesis platform enabled continuous flow synthesis of highly spherical and monodisperse Ag nanoparticles ranging from 5 to 80 nm.

4.2. Multiphase Flow

4.2.1. Liquid-Liquid Segmented Flow

In addition to single-phase, liquid flow synthesis, L-L segmented flow format may also be utilized for the shape-controlled synthesis of various colloidal nanomaterials. L-L segmented flow systems may either use a reactive or an inert carrier phase. Compared to the single-phase flow, L-L segmented flow format can aid anisotropic growth through interfacial reactions and interfacial adsorption.[101–103] The former has been demonstrated by Kulkarni et al. for the anisotropic growth of Au nanostructures in a L-L segmented flow microreactor.[102] The L-L segmented flow in this study consisted of a reducing agent in the organic phase and tetrachloroauric acid ($HAuCl_4$) in the aqueous phase, as generalized in **Figure 5**A. By varying the concentration of a surfactant (cetyltrimethylammonium bromide, CTABr) added to the aqueous phase, different morphologies with narrow shape distributions could be obtained. However, when identical CTABr concentrations were used in a single-phase system, wider shape distributions were observed. Shape variations were also found to be correlated to the hydrodynamics of the system. Hexagonal (plate-like) shapes could be preferentially grown by changing the reactant wall from hydrophobic to hydrophilic, which changed the dispersed phase from aqueous to organic. In this study, the growing nanostructures existed only in one phase as shown in Figure 5A. However, in L-L flow systems without surfactants or precursor mixing zones, nanoparticle seeds can be adsorbed at the continuous-dispersed phase interface. The effects of this interfacial adsorption were studied by Zhang et al. by using an oil-water segmented flow in a tube-based microfluidic reactor.[103] When Ag seeds accumulated at the oil-water interface, Ag octahedra and Ag-Au nanocups were produced via seeded growth and galvanic reactions, respectively (Figure 5BII). In the interfacial adsorption seeded growth synthesis, self-nucleation in the aqueous phase also resulted in small Ag nanoparticles. Polydispersity and shape variations could therefore be mitigated by the suppression of interfacial adsorption through the addition of a surfactant.

Outside of possible interfacial adsorption effects, the use of an inert carrier phase is largely beneficial not only to improve mixing due to formation of axisymmetric recirculation patterns within the plugs/slugs (Figure 1A) but also to reduce fouling. Using microscale L-L segmented flow format, shown in Figure 5C panel I, Niu et al. produced shape and size-controlled noble-metal nanocrystals with uniform morphologies (Figure 5CII–V).[104] The in-flow synthesized palladium (Pd) nanocube edge length was tuned by adjusting the ratio of Pd salt precursor to capping agent (Figure 5CII,III). Pd octahedra of larger sizes could be produced from Pd nanocubes via seed-mediated growth (Figure 5CV). The utilization of a silicone oil carrier phase (which removed fouling) enabled multiple (>10 times) operation of the microreactor without any major issues. Capitalizing on the silicone wetting phase a porous polytetrafluoroethylene (PTFE) tube-based separation unit was integrated after the cooling stage to remove the silicone oil from the reactant phase. Following the online L-L separation module, a cross-flow filtration module was used to collect Pd nanoparticles with enhanced efficiency compared to offline centrifugation. The combination of separation and filtration modules introduced in this microfluidic platform may further enable the application of shape-controlled flow syntheses of colloidal nanomaterials to industrial scale-automated systems.

In addition to continuous synthesis, microscale L-L segmented flow systems have enabled the high-throughput shape evolution screening of emerging colloidal nanomaterials, including inorganic and hybrid metal halide perovskites. Lignos et al., developed and utilized a temperature-controlled, droplet microfluidic platform integrated with an online PL monitoring module to elucidate the dynamics of halide segregation and nanocube and nanoplatelet formation during the synthesis of colloidal formamidinium lead halide (Cl/Br) perovskite nanostructures.[105] A comprehensive screening of key colloidal synthesis parameters, including ligand, cation, and halide composition as well as the synthesis temperature revealed the experimental boundaries in which nanoplatelet formation were in favor of nanocubes, thereby attaining tunable emissions spanning 440 to 515 nm, presented in Figure 5D. Furthermore, a maximum Cl to total halide threshold of 40% was identified for producing colloidally stable emitting nanocrystals, where all nanocrystals with Cl content exceeding this boundary underwent rapid halide ion segregation and an emission shift and/or reduction in the PL intensity.

In combination with single-phase microfluidic synthesis systems, L-L segmented flow systems have also been utilized to control morphology by separating nucleation and growth stages. One example includes a multistep microfluidic reactor introduced by Duraiswamy and Khan for the seedless synthesis of anisotropic gold nanocrystals, depicted in Figure 5E.[106] Au nanoparticle seeds were generated in the single-phase stage of the multistep microfluidic platform and subsequently injected via a four-way fluidic junction, along with aqueous growth precursor streams, into a cross-flow silicone oil stream to form

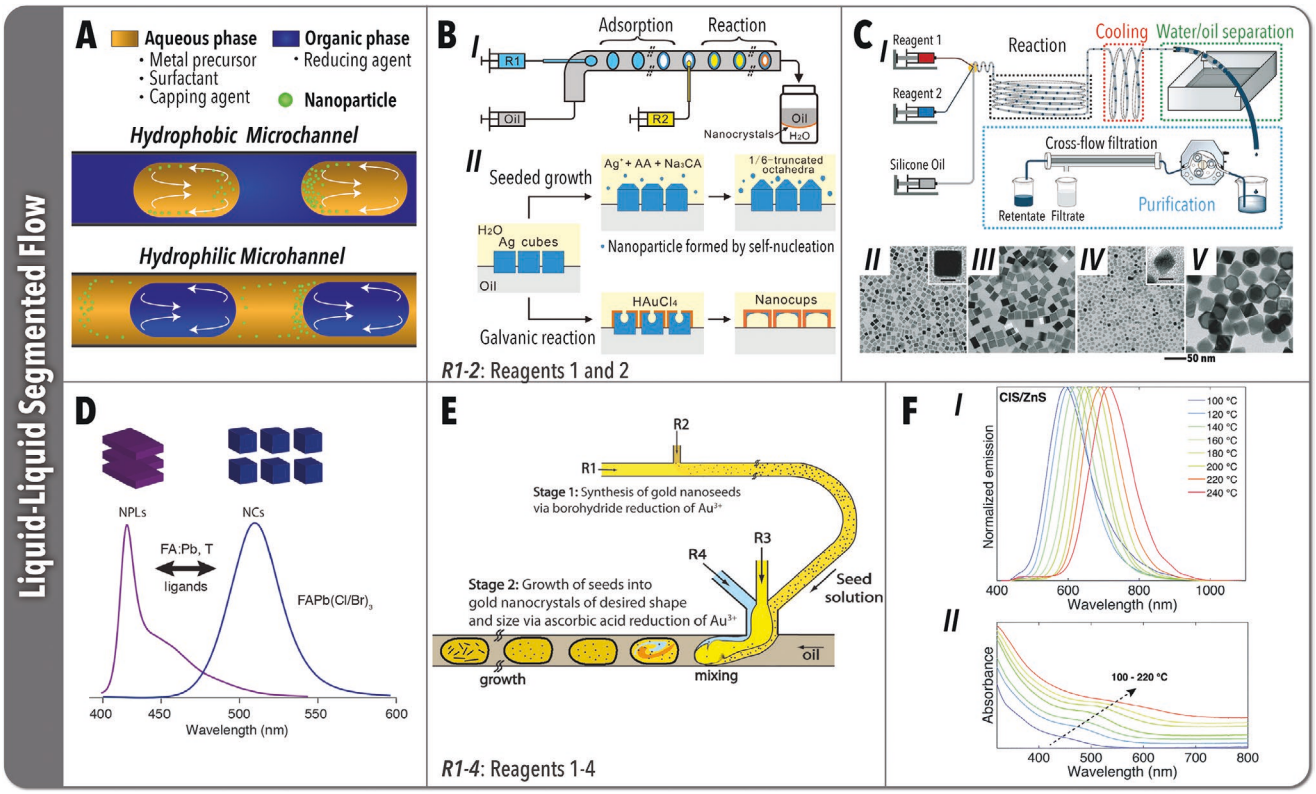

Figure 5. A) Illustration depicting microchannel wettability-dependent nanoparticle accumulation during Au nanoparticle growth discussed by Kulkarni et al.[102] The wettability of the microchannel was found to affect Au nanoparticle morphology, where hydrophobic and hydrophilic microreactors resulted in heterogeneous and uniform hexagonal shapes, respectively. B) (I) Illustration of the developed tube-based microfluidic reactor by Zhang et al. using the L-L segmented flow format for the interfacial adsorption assisted growth of anisotropic materials. (II) Schematic illustration of the interfacial adsorption and growth of Ag octahedra and Au-Ag (gold-silver alloy) nanocups. Adapted with permission.[103] Copyright 2014, American Chemical Society. C) (I) Schematic of the multistage, tube-based microfluidic platform developed by Niu et al. for the controlled in-flow synthesis of Pd nanostructures followed by continuous reactive phase extraction through permeable PTFE tubing. Tuning of precursor compositions and reaction temperatures enabled size controlled synthesis of Pd (II, III) nanocubes and (IV,V) nanooctahedra without offline phase separation. Adapted with permission.[104] Copyright 2018, American Chemical Society. D) Representation of the microfluidic high-throughput screening of colloidal $FAPb(Cl_{1-x}Br_x)_3$ nanocrystal shape evolution using a tube-based microfluidic reactor integrated with an online PL monitoring module by Lignos et al. Reproduced with permission.[105] Copyright 2018, American Chemical Society. E) Schematic illustration of the dual-stage continuous-flow microreactor developed by Duraiswamy and Khan for in-flow colloidal synthesis of anisotropic Au nanocrystals. Reproduced with permission.[106] Copyright 2013, Wiley-VCH. F) Online (I) PL and (II) absorption spectroscopy monitoring of $CuInS_2$/ZnS core–shell QDs as a function of core synthesis stage temperature by Yashina et al. Adapted with permission.[107] Copyright 2016, The Royal Society of Chemistry.

monodispersed L-L segmented flow in a microfabricated microreactor (polydimethylsiloxane). Such a multistage microfluidic reactor not only meets the benefits of one-pot batch syntheses but also provides finer growth control by decoupling the spatiotemporal overlap of seed generation and growth stage. In addition, a deionized water stream was added to the dispersed phase before segmentation to dilute the Au seed solution. By adjusting the water, gold salt/surfactant, and growth reagent flow rates, the relative concentrations of Au^{3+}, shape directing agent (Ag^+), and surfactant could be adjusted to modify Au nanocrystal morphology. The necessity of separating the seed and growth stages for anisotropic Au nanocrystal growth was demonstrated by a control experiment in which seed synthesis and growth reagents were combined at the same location and time, which resulted in no nanoparticle formation. Using offline UV–vis absorption spectroscopy, it was also determined that under the residence times used in stage one (≈90 s), incomplete seed growth occurred.

Similar to the seeded growth colloidal synthesis of anisotropic nanocrystals, core–shell nanocrystal syntheses also require multistep reactions. Although, compared to the single-phase microfluidic flow format, direct injection in microscale L-L segmented flow is a complicated task, the benefits of precision dosing can outweigh the challenges of multiphase injection. Such controlled and uniform multistep dosing, which may be attributed to isolated reactive phases and enhanced mixing in L-L segmented flow, has been demonstrated to result in improved core–shell nanostructures. Yashina et al. synthesized core/shell copper indium sulfide ($CuInS_2$)/zinc sulfide (ZnS) QDs in a two-stage microfluidic reactor utilizing L-L segmented flow format, where both $CuInS_2$ cores and ZnS shells were grown continuously in-series. ZnS shells were grown by direct injection of shell precursors into the reactive phase droplets containing $CuInS_2$ core QDs.[107] Online PL measurements were utilized for the continuous monitoring of the optical properties of the in-flow synthesized nanostructures

before and after shell growth as a function of precursor composition and synthesis temperature. Demonstrated by the emission and absorption spectra collected for varying core synthesis stage temperatures, the $CuInS_2$ QD core size could be independently controlled (Figure 5FI,II). Utilizing the developed two-stage microfluidic synthesis strategy, $CuInS_2$/ZnS core/shell QDs with tunable emissions (580–760 nm), moderate quantum yields (55%), and relatively low emission full-width at half-maximums (90–95 nm) were attained.

The synthesis of high-quality colloidal heterostructures in L-L flow reactors is made feasible not only from enhanced reaction control but also from enhanced reaction kinetics. By decreasing reaction times, the synthesis of air- and temperature-sensitive nanomaterials may be used in multistage reactions, such as the synthesis of colloidal core–shell materials. Cobalt-nickel core–shell MOFs created by sequential hydrothermal synthesis in a two-stage L-L microfluidic reactor were synthesized in 10 min, a dramatic reduction compared to 72 h required in conventional batch routes.[108] Because of the reduced heating time, the cobalt-benzene-1,3,5-tricarboxylate (Co_3BTC_2) MOF cores retained their crystalline properties after Ni_3BTC_2 shell growth. The use of segmented flow formats can, therefore, be used to synthesize novel nanomaterials due to the stability of synthesis intermediates at reduced reaction times.

4.2.2. Gas-Liquid Segmented Flow

Among adsorbates, those which are both facet-specific growth inhibitors and reducing agents, such as carbon monoxide (CO), have become a topic of focus in shape-controlled colloidal nanomaterial growth.[96] Batch colloidal syntheses employing such surface modifiers in the gas phase, termed gas reducing agent in liquid solution (GRAILS), have exhibited the shape-controlled synthesis of various metal nanostructures, including Pt-alloy and Pt icosahedra, and Pt octahedra.[109–111] Although tremendous progress has been made to parameterize shape control in GRAILS synthesis routes, poor control over G-L mass transfer and heating rates has limited their ability to produce uniform colloidal nanocrystals at high throughputs. Building upon the foundation laid by GRAILS synthesis, several gas-liquid segmented flow colloidal synthesis routes have recently been developed for the shape-controlled synthesis of metal and metal-oxide nanocrystals.[112–114] The generalized components of each phase in G-L segmented flow synthesis of colloidal nanocrystals are depicted in **Figure 6**A. Because of the high degree of kinetic control, accelerated heat and mass transfer rates (decreased reaction times), and reduced hazardous gas volumes, microscale G-L segmented flow format can realize the full potential of biphasic shape-controlled colloidal nanomaterial growth.

The unique advantages of G-L segmented flow format for controlled synthesis of colloidal nanomaterials have been demonstrated in a study by Sebastian et al., where a G-L microfluidic platform was utilized to synthesize Pd nanorods and nanosheets as well as Pt nanocubes with controlled morphologies.[114] The utilized two-stage silicon/pyrex microfluidic reactor consisted of a cooled passive mixing zone to promote microscale mixing of precursors without nucleation, followed by a heated reaction zone. Within this study, nanostructure shapes could be controlled by adjusting the gas phase between the reducing (CO), oxidizing (oxygen, O_2), and inert (nitrogen, N_2) gases as shown in Figure 6BI–IV. Using CO as the gas phase in the G-L segmented flow, Pd triangular nanosheets were synthesized at temperatures as low as 35 °C and residence times as low as 150 s. Shape control at higher temperatures was enabled by the addition of tetradecyltrimethylammonium bromide (TTABr) in combination with an aprotic solvent (dimethylformamide) which enhanced TTABr solubility to reduce fouling. Under the latter condition, temperature effect studies on Pd nanostructure morphology were conducted. By increasing the temperature between 50 and 100 °C, it was found that hexagonal Pd nanosheets could be obtained due to higher CO reduction rates and decreased CO coverage. UV–vis absorption spectroscopy was used to correlate shifts in surface plasmon resonance peaks to the synthesis temperature

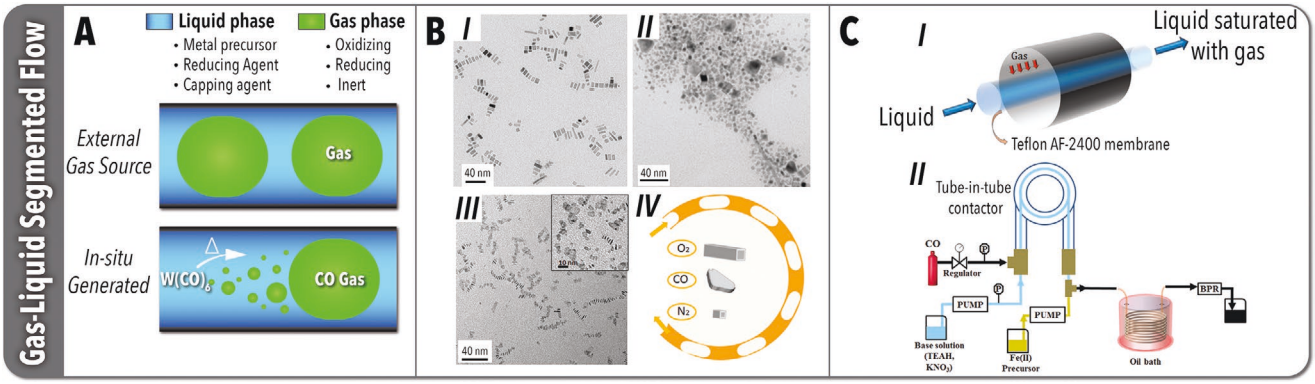

Figure 6. A) Illustration depicting microscale G-L flow synthesis of metal and metal oxide nanoparticles with (top) an external gas source acting as an oxidizing or reducing agent and/or inert carrier phase and (bottom) in situ generated gas reducing agent and carrier phase (CO) presented by Niu et al.[112] B) TEM images of the different in-flow obtained Pd morphologies by Sebastian et al. using G-L segmented flow microreactor with (I) O_2 (nanorods), (II) N_2, and (III) CO (nanosheets). Pd and Pt nanostructures were found to be controlled by temperature as well as liquid and gas-phase compositions. Adapted under the terms of the Creative Commons CC-BY license.[114] Copyright 2016, The Royal Society of Chemistry. C) (I) Tube-in-tube gas-liquid contactor used by Panariello et al. for the saturation of heptane and base solution streams with H_2 and CO, respectively, (II) CO-saturated single-phase flow reactor schematic for the CO-aided synthesis of iron oxide nanoparticles. Adapted under the terms of the Creative Commons CC-BY license.[115] Copyright 2020, The Authors, published by MDPI.

and Pd nanosheet edge lengths, demonstrating the potential for online optical absorption spectroscopy to be used in the high-throughput screening of shape-controlled colloidal metal nanostructure synthesis routes in flow. In addition to CO, O_2 was also utilized as the gas phase in the microscale G-L segmented flow reactor for the shape-controlled colloidal synthesis of Pd nanorods via anisotropic oxidative etching. Unlike batch methods, O_2 etching could be controlled to tune nanorod aspect ratios by tuning the G-L mass transfer rates via changing O_2 to liquid feed ratios.

Precise shape control similar to that applied in the microscale G-L segmented flow synthesis platform developed by Sebastian et al.[114] has also been demonstrated in tube-based microfluidic reactors toward the shape-controlled production of colloidal metal oxide nanostructures. Notably, a simple PTFE tube-based, two-stage G-L segmented flow microreactor was used by Larrea et al. to produce iron-oxide magnetic nanoparticles with tunable crystalline structures.[113] The first stage of this microfluidic platform used ultrasound waves to enhance mixing between solution phases. Next, the heated growth stage introduced the inert, oxidizing, or reducing gas phase via a Y-junction, resulting in the formation of G-L segmented flow. Because of the increased mass and heat-transfer rates, coupled with small slug sizes, gas phase and temperature-dependent iron oxide morphologies were obtained at residence times unparalleled in batch synthesis. For example, this study used hydrogen (H_2) gas as a reductant to produce pure phase magnetite at a residence time of 60 s, substantially lower than the reported hour-long batch synthesis. The study also highlighted the feasibility of high-throughput synthesis by demonstrating excellent size and shape reproducibility between multiple runs and during extended operation periods (≈3 h).

Safer-by-design G-L segmented flow microreactors, in addition to the external gas source protocols discussed, may use in situ generated CO gas as the carrier phase and reductant, represented by the illustration in Figure 6A (bottom). Niu et al. used this strategy in a tube-based microfluidic synthesis of Pt-nickel (Ni) octahedra.[112] The CO source, tungsten hexacarbonyl ($W(CO)_6$), was dissolved with Pt(II) acetylacetonate and Ni(II) acetylacetonate in oleic acid, olelyamine, and benzyl ether. Upon reaching a heating zone of the microfluidic reactor, the $W(CO)_6$ decomposed, releasing CO gas which separated the reactant solution into uniform droplets. Utilizing this G-L microfluidic synthesis strategy, rather than changing the external gas flow rate, slug sizes could be varied by adjusting the concentration of $W(CO)_6$ in the reactant stream.

4.2.3. Tubular Membrane-Based Flow Reactor

Recently, tube-in-tube flow reactors have been utilized to accelerate the rate of gas delivery to a liquid phase for gas-liquid synthesis of colloidal nanomaterials.[116] Gas-saturated liquid flow using the tube-in-tube flow reactor, compared to segmented G-L analogs, has greater potential for scale up since segmented flow stability requirements are eliminated. Panariello et al. used a two-stage flow synthesis platform comprised of a tube-in-tube G-L contactor followed by a heated PTFE flow reactor to synthesize iron oxide nanoparticles via coprecipitation method.[115] The G-L contactor stage consisted of a gas-permeable Teflon tube placed inside a PTFE tube, shown in Figure 6C panel I. Gas was flown on the outer annulus of the tube-in-tube contactor to saturate the liquid stream flowing within the inner Teflon tube. This flow reactor was used with two saturated liquid formats in the reactive stage: L-L segmented flow with H_2-saturated heptane as the continuous phase and single-phase liquid flow using a CO-saturated base solution (Figure 6CII). While H_2-saturated L-L flow aided the formation of high-purity magnetite/maghemite phase, spherical nanoparticle morphologies with high polydispersity were obtained, attributed to interfacial adsorption effects. To avoid interfacial adsorption effects on nanoparticle morphology, while maintaining phase purity, CO-saturated single-phase flow was used. Similar to the G-L segmented flow synthesis work by Larrea et al.,[113] at elevated temperatures CO acted as a reducing agent and only magnetite/maghemite phase nanoparticles with cuboidal morphology were obtained.

5. In-Flow Composition Control of Colloidal Nanomaterials

5.1. Nanomaterial Bulk Composition

Colloidal nanomaterials are particularly congruous with microfluidic synthesis technology due to their high degree of compositional variation. That is, the composition, and thus application, of heterogeneous colloidal nanomaterials can be tuned for the same reactants by controlling synthesis conditions including residence time, pressure, immobilization time, temperature, and precursor ratios. These readily accessible and precisely tunable synthesis conditions, such as in size- and shape-controlled synthesis, may be rapidly screened in microfluidic reactors, thereby accelerating the understanding of the key parameters controlling the physicochemical properties of colloidal nanomaterials. An emerging example of composition-controlled colloidal synthesis aided by flow synthesis strategies is the continuous flow synthesis of bimetallic catalytic nanoparticles.[117] When synthesized via coreduction in batch, stabilized bimetallic alloy-nanoparticles typically have compositional variation across a range of nanocrystal sizes. Because these compositional changes are poorly controlled and result in variations in selectivity and activity, the realization of bimetallic catalysts in industry has been impeded. Recently, a flow synthesis approach, which overcomes the downfalls of batch sol-immobilization synthesis, was demonstrated by Cattaneo et al.[117] for the continuous production and immobilization of Au-Pd alloy nanoparticles. By rapidly combining Pd and Au precursors and a reductant ($NaBH_4$) as well as quickly immobilizing the formed alloy nanoparticles in flow, Au-Pd nanoparticles with compositional homogeneity across a range of nanoparticle sizes were achieved (**Figure 7**AI,II). Conversely, the molar ratio of alloy nanoparticles can also be tuned while maintaining a constant size by adjusting the residence (reaction) time as shown in the continuous flow synthesis of Au-Ag alloy nanoparticles by Sun et al.[118] Using a heated PTFE capillary microreactor coupled with offline structural and spectral characterization techniques, Au-Ag alloy nanoparticle composition and size

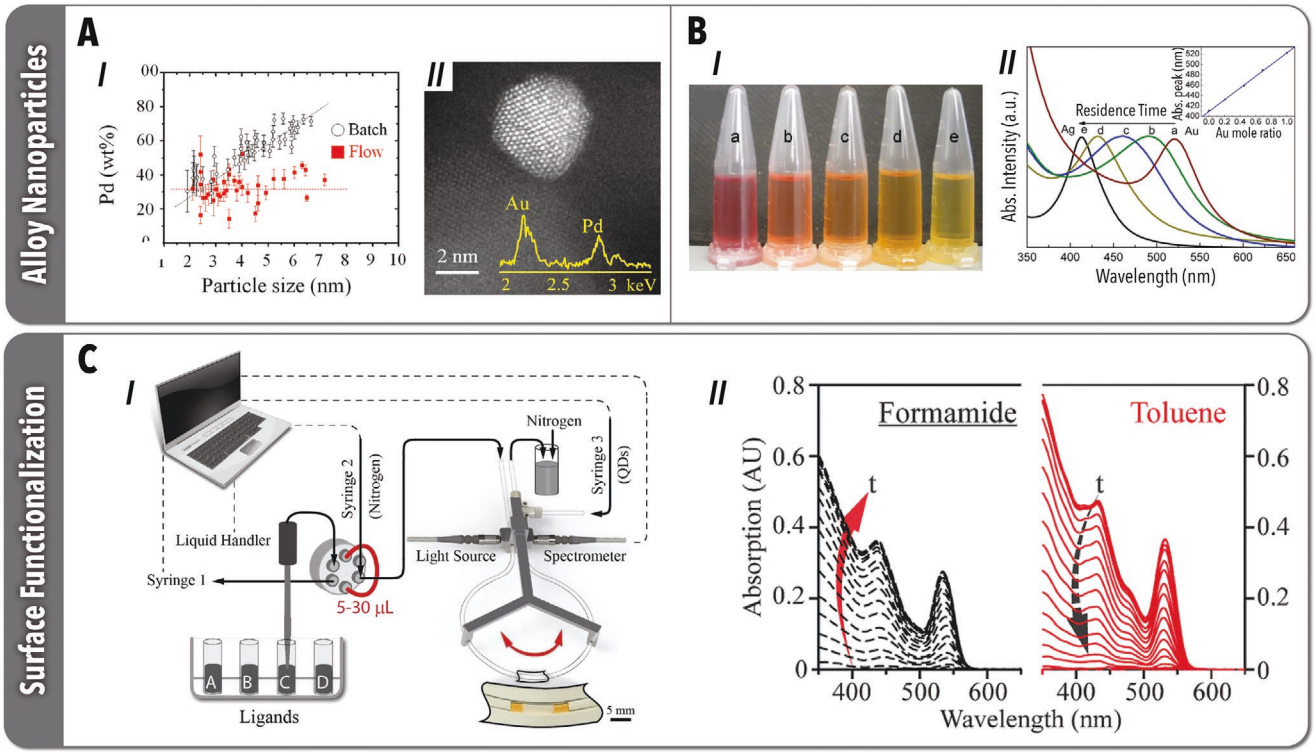

Figure 7. A) (I) Titania-supported AuPd alloy nanoparticle size versus composition for nanoparticles synthesized in a continuous millifluidic reactor compared to batch, as presented by Cattaneo et al.[117] Size and composition of alloyed nanoparticles were measured using (II) XEDS. Compared to batch, in-flow synthesized AuPd alloy nanoparticles displayed compositional homogeneity across a wide range of particle sizes. Adapted with permission.[117] Copyright 2017, The Royal Society of Chemistry. B) Pictures of (I) Au (a), Au-Ag (b–d), and Ag (e) colloidal nanoparticles synthesized utilizing a PTFE capillary microreactor developed by Sun et al.[118] (II) The SPR absorption peak can be tuned by changing the residence time, and thus composition, of the (III–IV) alloy nanoparticles. Adapted under the terms of a Creative Commons Attribution 2.0 International License.[118] Copyright 2017, The Authors, published by Springer Nature. C) (I) Schematic illustration of the single-droplet oscillatory flow reactor developed by Shen and Abolhasani et al. for the online study of biphasic ligand exchange reactions using OA- and ODPA-capped CdSe QDs. (II) The concentration of CdSe in each phase, and thus extent of ligand exchange, monitored online via the absorbance value at 350 nm. Adapted with permission.[122] Copyright 2017, Wiley-VCH.

were evaluated as a function of residence time (Figure 7BI,II), synthesis temperature, and molar ratio of Au and Ag reactants. In addition, changes in plasmon resonance absorption peaks were correlated to changes in Au/Ag alloy molar ratio. Through a precise control of temperature and residence time, this microfluidic synthesis platform demonstrated the potential of fluidic systems to rapidly identify optimal synthesis conditions which increase throughput, while maintaining size and compositional homogeneity.

Although optical absorption spectroscopy can be used to study compositional variations in nanomaterials, more robust characterization techniques which can provide information on oxidation state, local order, and coordination number are also available, specifically XAS. However, because many of such characterization tools require acquisition times orders of magnitude higher than reaction rates, they are impractical for kinetic studies of colloidal syntheses with fast formation kinetics ($\ll$1 s). Thus, there has been a disjunction between emerging nanomaterials (which typically involve reaction time scales significantly lower than their bulk analogues) and advanced characterization tools. However, since reaction time in flow is a function of the microreactor length, these characterization methods can be used in flow syntheses with fast kinetics simply by changing the sampling area to different points along a microfluidic reactor. With the emergence of microfabricated reactors tailored to online XAS and extended X-ray absorption fine structure (EXAFS) analysis, this advantage has been exploited toward kinetic studies of ultrafast reactions via composition analysis. Chan et al.[119] demonstrated the use of online XAS for detailed kinetic studies of CdSe to Ag_2Se nanocrystal cation exchange reactions in flow using a three-stage silicon-based microreactor. The microfluidic reactor consisted of inlet channels for Ag^+ and CdSe reagents, followed by a flow-focusing mixing channel and an observation channel. The dimensions of the observation channel were made wider than the mixing channel to accommodate the X-ray spot and an aligned nitride window. Using (residence) time-resolved XAS spectra, the fractional conversion of CdSe to Ag_2Se as a function of time was measured online, revealing insights into the possible mechanisms of $CdSe/Ag^+$ cation exchange reactions.

5.2. Surface Functionalization

Changes in composition via surface functionalization may also be used to change the optical properties and applications

of colloidal nanomaterials. For example, surface functionalization of semiconductor QDs via ligand exchange reactions can increase charge transfer between QDs and improve their solubility in polar solvents.[120,121] Heterogeneous ligand exchange reactions are well-controlled alternatives to homogeneous-phase and postdeposition reactions. Until recently, a detailed kinetic understanding of heterogeneous ligand exchange reactions was limited by the labor-intensive phase separation and purification required for offline spectroscopic measurements. Using a single-droplet oscillatory microfluidic reactor with online absorption spectroscopy, Shen and Abolhasani et al.[122] studied the biphasic ligand exchange kinetics of oleate (OA)- and octadecylphosphonic acid (ODPA)-capped CdSe QDs (in toluene) with sulfide anions (in formamide), shown in Figure 7C panel I. Because of a difference in the relative velocity of the engulfed polar phase (formamide) and the wetting phase (toluene), the polar phase displaced to the front of the biphasic droplet at the ends of the horseshoe-shaped microfluidic reactor, allowing for straightforward delineation of each phase for online UV–vis absorption analysis. By monitoring the concentration of CdSe in each phase—obtained from the online UV–vis absorption data, as shown in Figure 7C panel II—kinetic curves for different phase volume ratios were obtained demonstrating that the biphasic ligand-exchange reaction was not mass transfer controlled. In addition, a ligand exchange mechanism was proposed based on the evolution of band-edge extinction peak positions as a function of time. Based on known peak shift changes correlated with the dissociation of Z-type ligands (blueshift) and X-type ligands (redshift), the leaving order was found to begin with be X-type oleate and Z-type Cd-phosphonate for OA and ODPA-capped CdSe QDs, respectively.

Outside of comprehensive kinetic studies, microfluidic reactors have also been employed for the continuous and material-efficient surface functionalization of nanomaterials. Uson et al.[123] functionalized Au nanorods in flow with poly(ethylene glycol) (PEG), a common surface modifier used to stabilize Au nanostructures as well as reduce their cytotoxicity for biomedical application. Using a multistep microfluidic reactor, Au nanorods were grown by seeded growth and PEGylated in a continuous flow process. PEGylation of Au nanorods in flow required two orders of magnitude less PEG compared to batch, which was estimated to result in dramatic cost reductions based on PEG making up ≈69% of the cost of raw materials used to produce Au-PEG nanorods. Similar material and cost-efficient benefits were obtained by Gomez et al.[124] for the continuous production and PEGylation of hollow Au nanoparticles in a tube-based microfluidic reactor and in a scaled-up tube-based millifluidic reactor. Beyond material and cost efficiency, the reduction in PEG required in both processes also saved time by eliminating purification steps required for excess PEG in solution.

6. Autonomous Colloidal Nanomaterial Synthesis

The facile access to multitude of process parameters along with online, streamlined data acquisition (nanomaterial properties), make microfluidic systems well suited for integration with existing and emerging feedback controllers and reaction optimization algorithms. Process controllers are especially useful for sustained parameter modulation in syntheses which require extended synthesis times as well as in scaled-out, end-to-end manufacturing. Controllers which have been integrated into microfluidic nanomaterial synthesis platforms primarily use proportional-integral-derivative control (e.g., Chan et al. for temperature-controlled, microfluidic synthesis of CdSe QDs)[125] and fuzzy logic algorithms (e.g., Kerr et al. for microfluidic synthesis of $CsPbBr_3$ QDs to simultaneously tune flow velocity and reactive slug length).[126]

Single-phase fluid delivery systems able to attain high levels of precision are available off-the-shelf and may be integrated into in-flow colloidal nanomaterial syntheses without extensive prior knowledge. Multiphase fluid velocity tuning strategies are, however, less commonly used and are more complex than the simple flow rate tuning of single-phase flow formats. Due to the dynamic nature of microscale G-L and L-L segmented flow formats (e.g., compression of gaseous phases, physically driven phase changes), they are highly sensitive to invasive measurement methods. Consequently, the primary method for monitoring multiphase flow systems has been through low-cost optical sensors,[127] which have been integrated into process controllers through strategies such as slug counting.[126] While multiphase flow control methods are in the early stages of application in colloidal nanoscience studies, modest development of these optical monitoring and control strategies would alleviate this technical barrier at a negligible equipment cost. Similarly, the physical components of most temperature control systems (thermocouple, energy source, and controller) are commercially available and amenable to automated process controllers. Moreover, they may be easily integrated into a larger control system using algorithms freely available in most programming languages and software packages (e.g., Python and LabVIEW).

Building upon the continuous tuning of the accessible synthesis parameter space, autonomous robotic experimentation in flow can be achieved through the integration of online analytical methods with the emerging AI-based experiment selection algorithms. Capitalizing on high sampling rates and low chemical requirements, such AI-guided flow synthesis platforms are powerful intelligent experimentation tools for rapid parameter space mapping, synthesis optimization, and application-guided formulation discovery. Widespread integration of autonomous systems in colloidal nanoscience research, would therefore, significantly accelerate the discovery, synthesis, and process–structure–property mapping of the emerging colloidal nanomaterials in energy and chemical technologies. However, despite a growing number of demonstrations in nanocrystal syntheses, fully autonomous reactors still possess a significant number of barriers to their proliferation. An effective autonomous flow reaction optimizer cannot be attained without first understanding and applying six key components: 1) The entirety of the system hardware—including temperature control, reagent delivery, and process/material characterization probes—must be fully automated; 2) Online process/material characterization modules must provide accurate and physically validated data; 3) Data analytics on relevant parameters must be automated through unassisted feature detection/extraction algorithms; 4) The microfluidic nanomaterial synthesis platform must access

a relevant range for each experimental parameter at a relatively low sampling variability; 5) The microfluidic platform must be able to operate continuously for the entire duration of the exploration/optimization process; 6) The objective parameter must be sufficiently correlated to the controlled input variables and subsequently optimized through an experiment selection algorithm. Due to the complexity of each of these challenges, use of autonomous robotic experimentations in flow typically falls within a specialized area of research, but with appropriate propagation of the relevant information, these deterrents may be quickly lifted.

First, a baseline level of technical knowledge is required to design and assemble a microfluidic system. The fundamental principles toward building accurate and efficient microfluidic platforms, particularly low-cost tubular microreactors, have been extensively detailed in other publications and review articles.[46] Second, there is a need for user-friendly integrated hardware and data processing algorithms. While most equipment manufacturers offer simple plug-and-play communication devices and a number of measurement extraction strategies have been demonstrated,[128] using a collection of hardware and automatically analyzing the resulting data currently requires a background in process automation and computer language programming. Greater availability of fully integrated microfluidic control systems would undoubtedly reduce the initial barrier in autonomous colloidal synthesis studies. Finally, while integration of experiment selection algorithms with a microfluidic platform falls into the requisite prior knowledge in computer programming, the algorithms on their own have been extensively studied. Several fully developed experiment selection methods are available in a readily implementable format and have already been demonstrated in nanomaterial syntheses. Furthermore, a number of more recently developed AI-based experiment analysis and selection approaches have demonstrated a clear potential in accelerated colloidal synthesis studies.[129,130]

Open-source prepackaged optimization algorithms are accessible options for autonomous robotic experimentation in flow, and many of such algorithms have been already incorporated into microfluidic systems with notable success.[131,132] The earliest implementation of a self-guided nanoparticle synthesizer applied the open-source software package Stable Noisy Optimization by Branch and Fit[133] to tune the PL emission of CdSe QDs,[134] and in more recent work the same algorithms were integrated with a remote user interface and robotically handled offline circular dichroism spectroscopy measurements toward the intelligent synthesis of chiral perovskite nanocrystals[135]—shown in **Figure 8**A. Additionally, the Nelder–Mead simplex method[136] has been applied as an advanced process controller for the continuous nanomanufacturing of $CsPbBr_3$ QDs,[137] and covariance matrix adaption-evolutionary strategy[138] was recently used to tune the halide exchange of $CsPbBr_3$ QDs.[65]

Algorithms based on Gaussian process regressions (or Kriging) offer more available tuning parameters and facile selection flexibility than most prepackaged optimization algorithms, at the cost of greater implementation complexity. The use of Gaussian process-based experiment selection strategies has aided in the accelerated colloidal syntheses of CdSe, CdSeTe,[139] and multinary lead halide perovskite QDs[140]—shown in Figure 8B. Similarly, ensemble neural network-based algorithms seek to capture the extensive complexity of nanoparticle synthesis systems through modern advances in AI. While the strategy is in its infancy for colloidal nanoparticles, the use of neural network algorithms has recently been demonstrated for halide exchange reactions of $CsPbBr_3$ QDs[65]—shown in Figure 8C.

Ultimately, the most effective experiment selection strategy will depend on the nature of the colloidal synthesis routes and accessible parameter space. Gaussian process regressions are trained and applied at a far lower computational cost than current AI-based models; however, neural network algorithms may offer more robust experiment selection as well as access to more complex reaction spaces. The superior technique will likely change depending on the nanoparticles being formed and the utilized microfluidic system. Effectively identifying which experiment selection algorithms are more appropriate for each class of colloidal nanomaterials warrants extensive future study.

7. Summary and Outlook

In the scope of nanomaterial synthesis exploration and discovery, microfluidic reactors offer superior sampling efficiencies and kinetic control over flask-based reaction strategies. Such kinetic control can be coupled with online monitoring techniques for unparalleled insight to the evolution of colloidal nanomaterial properties over a wide range of reaction times. The simplicity of microfluidic platform automation allows for many of the presented flow syntheses to be used toward fully autonomous, self-optimizing colloidal syntheses. Because of the ability to have continuously controlled microreactor stages, as well as enhanced reaction kinetics, microfluidic platforms can also be used for the synthesis of next-generation nanomaterials previously unobtainable due to challenges with handling air- and temperature-sensitive intermediates. Moving toward nanomanufacturing strategies, microfluidics allows for the direct transfer of laboratory-scale studies to large-scale production through numbered up designs. Furthermore, small active reactor volumes (at least two orders of magnitude lower than equivalent batch reactors) facilitate safer-by-design nanomaterial production, allowing for the realization of shape-controlled synthesis employing hazardous volatile phases in high-throughput manufacturing.

The recent advances in the capabilities of modular microfluidic reactors make them a powerful strategy for the size, shape, and compositional-controlled synthesis of colloidal nanomaterials. While this progress report focused on the controlled synthesis of quantum, magnetic, and plasmonic inorganic nanomaterials, there are a growing number of next-generation colloidal nanomaterials which would benefit from precise control and accelerated high-throughput screening capabilities of microfluidic synthesis strategies. Among these materials are those which can be synthesized by interfacial reactions, including colloidal metal–organic frameworks[141] and carbon dots.[142] Due to increased mixing rates and a continuously replenished interface in multiphase microfluidic reactors, reaction times for interfacial-colloidal syntheses may be

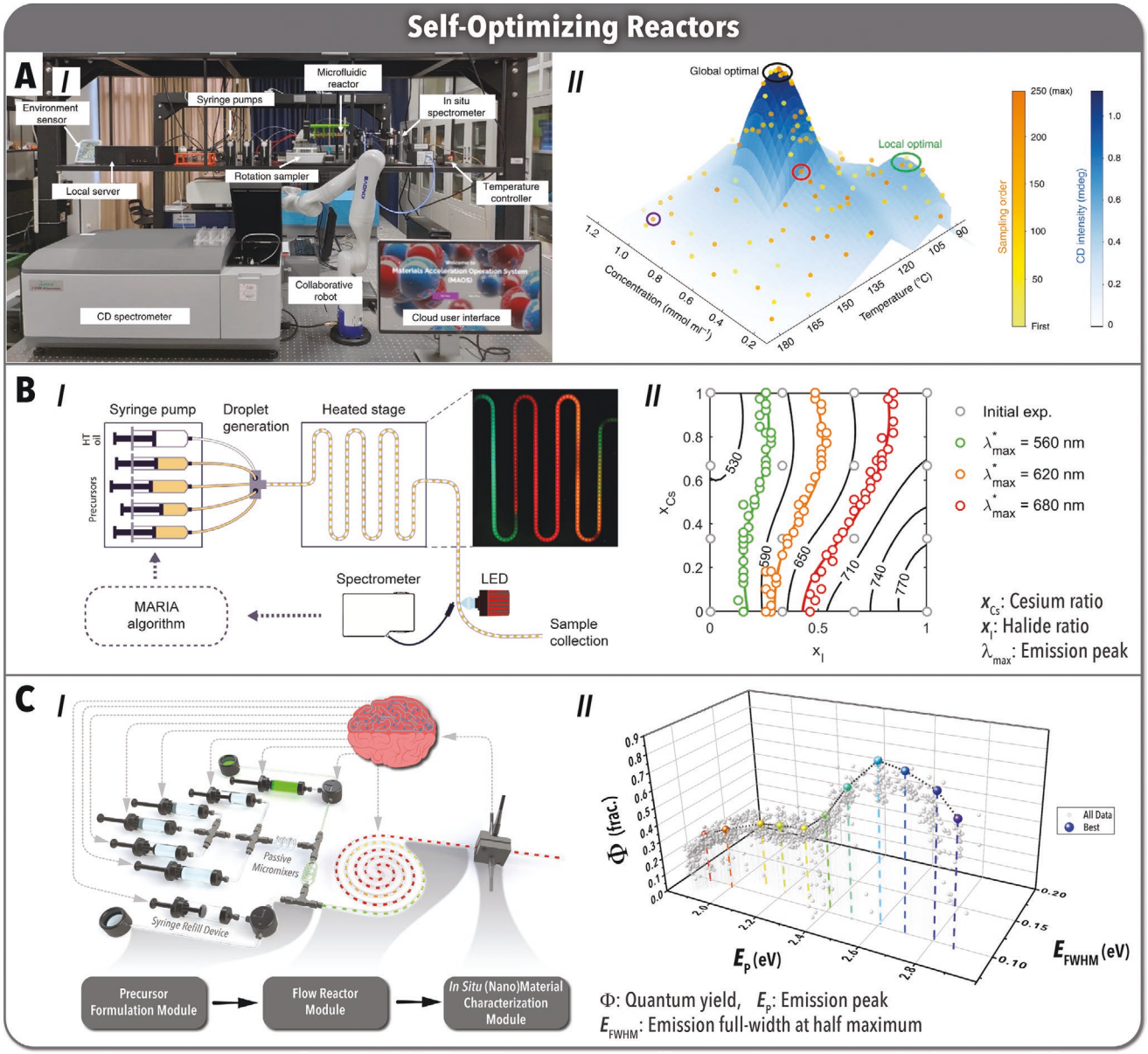

Figure 8. A) (I) Photograph of cloud interface, microfluidics, and robotic sample handler integrated into a perovskite nanocrystal synthesizer, as detailed in Li et al. Online absorption spectroscopy and robotically handled offline circular dichroism spectroscopy data were used in (II) Stable Noisy Optimization by Branch and FIT optimization algorithms. Apapted under the terms of a Creative Commons Attribution 4.0 International License.[135] Copyright 2020, The Authors, published by Springer Nature. B) (I) Illustration of the developed microfluidic system by Bezinge et al. integrated with the multiparametric automated regression kriging interpolation and adaptive sampling algorithm used to tune the emission wavelength of various multinary lead halide perovskite nanocrystals. (II) Iterative sampling results for three target emission peak wavelengths in a two parameter input space. Adapted with permission.[140] Copyright 2018, American Chemical Society. C) (I) Schematic illustration of the ensemble neural network guided Artificial Chemist, developed by Epps et al.,[65] which (II) applied an objective function to simultaneously optimize the quantum yield and polydispersity for eleven target emissions in the halide exchange of inorganic metal halide perovskite nanocrystals. Adapted with permission.[65] Copyright 2020, Wiley-VCH.

greatly reduced. Furthermore, materials which necessitate unit cell precision growth, such as low-dimensional perovskite nanostructures, will benefit from the superior control of colloidal synthesis parameters in microfluidic reactors over batch processes. Beyond size, shape, and composition-controlled synthesis of next-generation colloidal nanomaterials, nanomaterials with advanced structure–property relationships, such as those with strain-induced optical properties,[143] will also benefit from advanced fluidic synthesis strategies. Although the microfluidic syntheses of colloidal nanomaterials within some of these categories have been demonstrated and covered in recent reviews, there is an underexplored opportunity for the application of online characterization techniques toward fundamental kinetic studies.

As previously mentioned, the residence (reaction) time relationship of microfluidic reactors can be used to study reaction

kinetics typically too fast for online high-resolution characterization methods. For example, online small-angle and wide-angle X-ray scattering may be used with the microfluidic synthesis of MOFs, among many other materials in the rapidly growing library of porous nanostructures (such as zeolites and covalent–organic frameworks), toward understanding crystallization kinetics. Outside of nucleation and growth studies, additional opportunities include studying the degradation, annealing, and ripening kinetics of a wide range of colloidal nanomaterials. While these opportunities have been enabled by developments in microreactor designs amenable to online characterizations, recent progress has also been made in spectroscopic techniques used in flow. For example, differential detection photothermal spectroscopy has been applied by Maceiczyk and Hess et al.[87] to measure concentration in low volume and residence time droplets, overcoming pathlength and time resolution barriers of absorption spectroscopy. To overcome pathlength limitations of PL spectroscopy in high concentration samples, Epps et al. have introduced a reduced pathlength flow cell suitable for online PL quantum yield measurements of high PL materials without any dilution.[65] With such progress in online characterization techniques and microreactor designs, autonomous and self-optimizing fluidic systems may be realized—one of the greatest potentials of colloidal nanomaterial flow synthesis.

Existing self-optimizing microfluidic systems rely on temperature and reactant concentration tuning to optimize nanoparticles synthesis routes. While the capabilities of these technologies considerably alleviate the need for labor-intensive parameter screening, far greater opportunities arise from their development. In a manner similar to recent pioneering work in AI-assisted organic synthesis planning in flow reactors, autonomous nanoparticle reactors are ready to traverse into comprehensive compositional screening. The algorithms and platforms used to explore and optimize synthesis conditions may now be designed to incorporate the molecular features of available precursors into the experiment selection process. A self-optimizing fluidic system with a large variety of available precursors integrated with basic materials informatic algorithms would offer unprecedented, in both flow chemistry and nanoscience, colloidal synthesis exploration. Such a system would unlock a greater, and potentially unintuitive, breadth of information surrounding the mechanisms of shape, size, and composition-controlled colloidal nanoparticle syntheses, and it would result in new and higher performing nanomaterials.

Microfluidic reactor designs and their applications in colloidal nanomaterial syntheses have advanced significantly in recent years. The tools and strategies developed by microfluidic device engineers may be used to expound the mechanisms and unravel the synthesis space of a wide variety of colloidal nanomaterials at an efficiency and rate unattainable at any point in history. The key remaining challenge in implementing these systems toward higher quality nanomaterial design and production is unification of research efforts. Despite the advantages of microfluidic synthesis systems, most groundbreaking advances are nanomaterial syntheses, quality, and performance, still occur through flask-based experimentation. The skillset currently required to design and build a microfluidic synthesis screening system is largely independent of the understanding needed to design colloidal synthesis protocols at the forefront of innovation, and it is unrealistic to expect mastery of both from a single scientist. This challenge may be overcome by 1) promoting interdisciplinary efforts, where colloidal nanomaterial researchers may develop synthesis strategies from the ground up in tandem with microfluidic reactor engineers, and 2) reducing the barrier of entry for flow-based experimentation by creating comprehensive plug-and-play microfluidic synthesis and monitoring systems. Microfluidics holds incredible potential for understanding and improving the synthesis of colloidal nanomaterials. While many flow-based synthesis systems are regarded as novel, the greater scientific community will benefit from their advanced capabilities becoming conventional.

Acknowledgements

The authors gratefully acknowledge the financial support provided by the National Science Foundation (Award No. 1902702) and the UNC Research Opportunities Initiative (UNC-ROI) grant and North Carolina State University.

Conflict of Interest

The authors declare no conflict of interest.

Keywords

accelerated materials development, autonomous robotic experimentation, colloidal nanomaterials, microfluidics

Received: July 1, 2020
Revised: August 3, 2020
Published online: December 2, 2020

[1] S. Y. Lim, W. Shen, Z. Gao, *Chem. Soc. Rev.* **2015**, *44*, 362.
[2] J. Shen, Y. Zhu, X. Yang, C. Li, *Chem. Commun.* **2012**, *48*, 3686.
[3] X. Li, M. Rui, J. Song, Z. Shen, H. Zeng, *Adv. Funct. Mater.* **2015**, *25*, 4929.
[4] Y. Xia, X. Xia, H. C. Peng, *J. Am. Chem. Soc.* **2015**, *137*, 7947.
[5] Q. Li, S. Sun, *Nano Energy* **2016**, *29*, 178.
[6] J. Polte, *CrystEngComm* **2015**, *17*, 6809.
[7] J. Owen, L. Brus, *J. Am. Chem. Soc.* **2017**, *139*, 10939.
[8] C. B. Murray, C. R. Kagan, M. G. Bawendi, *Annu. Rev. Mater. Sci.* **2000**, *30*, 545.
[9] D. Astruc, F. Lu, J. R. Aranzaes, *Angew. Chem., Int. Ed.* **2005**, *44*, 7852.
[10] R. Narayanan, M. A. El-Sayed, *J. Phys. Chem. B* **2005**, *109*, 12663.
[11] X. Zhu, Y. Lin, Y. Sun, M. C. Beard, Y. Yan, *J. Am. Chem. Soc.* **2019**, *141*, 733.
[12] P. Couvreur, *Adv. Drug Delivery Rev.* **2013**, *65*, 21.
[13] O. C. Farokhzad, R. Langer, *ACS Nano* **2009**, *3*, 16.
[14] G. Reiss, A. Hütten, *Nat. Mater.* **2005**, *4*, 725.
[15] E. H. Sargent, *Nat. Photonics* **2012**, *6*, 133.
[16] V. K. Lamer, R. H. Dinegar, *J. Am. Chem. Soc.* **1950**, *72*, 4847.
[17] W. Ostwald, *Z. Phys. Chem.* **1990**, *34*.
[18] M. A. Watzky, R. G. Finke, *Chem. Mater.* **1997**, *9*, 3083.
[19] M. Niederberger, H. Cölfen, *Phys. Chem. Chem. Phys.* **2006**, *8*, 3271.
[20] H. Zheng, R. K. Smith, Y. W. Jun, C. Kisielowski, U. Dahmen, A. P. Alivisatos, *Science* **2009**, *324*, 1309.

[21] S. G. Kwon, T. Hyeon, *Small* **2011**, *7*, 2685.
[22] E. E. Finney, R. G. Finke, *J. Colloid Interface Sci.* **2008**, *317*, 351.
[23] N. T. K. Thanh, N. Maclean, S. Mahiddine, *Chem. Rev.* **2014**, *114*, 7610.
[24] J. S. Barea, J. Lee, D. K. Kang, *Micromachines* **2019**, *10*, 412.
[25] T. Yang, J. Choo, S. Stavrakis, A. de Mello, *Chem. - Eur. J.* **2018**, *24*, 12078.
[26] Q. Zhong, H. Ding, B. Gao, Z. He, Z. Gu, *Adv. Mater. Technol.* **2019**, *4*, 1800663.
[27] A. Webster, J. Greenman, S. J. Haswell, *J. Chem. Technol. Biotechnol.* **2011**, *86*, 10.
[28] G. M. Whitesides, *Nature* **2006**, *442*, 368.
[29] J. N. Lee, C. Park, G. M. Whitesides, *Anal. Chem.* **2003**, *75*, 6544.
[30] K. F. Jensen, *MRS Bull.* **2006**, *31*, 101.
[31] K. P. Prathish, R. C. Carvalho, C. M. A. Brett, *Electrochim. Acta* **2016**, *187*, 704.
[32] J. P. Rolland, R. Michael, V. Dam, D. A. Schorzman, S. R. Quake, J. M. Desimone, *J. Am. Chem. Soc.* **2004**, *126*, 2322.
[33] S. Kubendhiran, Z. Bao, K. Dave, R. S. Liu, *ACS Appl. Nano Mater.* **2019**, *2*, 1773.
[34] V. Kumar, H. A. Fustér, N. Oh, Y. Zhai, K. Deshpande, M. Shim, P. J. A. Kenis, *ChemNanoMat* **2017**, *3*, 204.
[35] T. W. Phillips, I. G. Lignos, R. M. Maceiczyk, A. J. Demello, J. C. Demello, *Lab Chip* **2014**, *14*, 3172.
[36] Y. Xin, S. Peng, J. Chen, Z. Yang, J. Zhang, *Chin. Chem. Lett.* **2020**, *31*, 1448.
[37] Z. Liu, J. Zhu, C. Peng, T. Wakihara, T. Okubo, *React. Chem. Eng.* **2019**, *4*, 1699.
[38] Y. He, S. Hu, T. Han, X. Chen, Y. Yu, T. Li, W. Zhu, G. Ouyang, *ACS Omega* **2019**, *4*, 9198.
[39] K. B. Mogensen, K. Kneipp, *J. Phys. Chem. C* **2014**, *118*, 28075.
[40] A. Veamatahau, B. Jiang, T. Seifert, S. Makuta, K. Latham, M. Kanehara, T. Teranishi, Y. Tachibana, *Phys. Chem. Chem. Phys.* **2015**, *17*, 2850.
[41] A. A. Tiba, A. V. Tivanski, L. R. MacGillivray, *Nano Lett.* **2019**, *19*, 6140.
[42] A. Sashchiuk, D. Yanover, A. Rubin-Brusilovski, G. I. Maikov, R. K. Čapek, R. Vaxenburg, J. Tilchin, G. Zaiats, E. Lifshitz, *Nanoscale* **2013**, *5*, 7724.
[43] G. Collins, J. D. Holmes, *Adv. Mater.* **2016**, *28*, 5689.
[44] D. Vasudevan, R. R. Gaddam, A. Trinchi, I. Cole, *J. Alloys Compd.* **2015**, *636*, 395.
[45] I. G. Lignos, R. C. R. Wootton, A. J. DeMello, B. M. Stone, *Encyclopedia of Biophysics*, Springer, Berlin **2013**, pp. 2300–2306.
[46] L. J. Pan, J. W. Tu, H. T. Ma, Y. J. Yang, Z. Q. Tian, D. W. Pang, Z. L. Zhang, *Lab Chip* **2018**, *18*, 41.
[47] A. Günther, K. F. Jensen, *Lab Chip* **2006**, *6*, 1487.
[48] R. L. Hartman, J. P. McMullen, K. F. Jensen, *Angew. Chem., Int. Ed.* **2011**, *50*, 7502.
[49] N. Convery, N. Gadegaard, *Micro Nano Eng.* **2019**, *2*, 76.
[50] D. T. Chiu, A. J. Demello, D. Di Carlo, P. S. Doyle, C. Hansen, R. M. Maceiczyk, R. C. R. Wootton, *CHEMPR* **2017**, *2*, 201.
[51] D. E. Angelescu, D. Siess, *Proc. IEEE Sens.* **2005**, 175.
[52] L. Peng, M. Yang, S. S. Guo, W. Liu, X. Z. Zhao, *Biomed. Microdevices* **2011**, *13*, 559.
[53] K. Wang, Y. C. Lu, J. H. Xu, G. S. Luo, *Langmuir* **2009**, *25*, 2153.
[54] X. Casadevall i Solvas, A. De Mello, *Chem. Commun.* **2011**, *47*, 1936.
[55] T. N. Wong, C. Wang, H. Li, Y. Gao, N. T. Nguyen, C. Yang, K. T. Ooi, *Encyclopedia of Microfluidics and Nanofluidics*, Springer, New York **2013**, pp. 1–21.
[56] Gaurav, V. Shankar, *Phys. Fluids* **2013**, *25*, 014104.
[57] C. E. Stanley, R. C. R. Wootton, A. J. DeMello, *Chimia* **2012**, *66*, 88.
[58] Y. Li, R. K. Reddy, C. S. S. R. Kumar, K. Nandakumar, *Biomicrofluidics* **2014**, *8*, 054125.
[59] R. G. Antony, M. S. G. Nandagopal, N. Sreekumar, S. Rangabhashiyam, N. Selvaraju, *Bull. Chem. React. Eng. Catal.* **2014**, *9*, 207.
[60] J. R. Burns, C. Ramshaw, *Lab Chip* **2001**, *1*, 10.
[61] R. W. Epps, K. C. Felton, C. W. Coley, M. Abolhasani, *Lab Chip* **2017**, *17*, 4040.
[62] F. Destremaut, J. B. Salmon, L. Qi, J. P. Chapel, *Lab Chip* **2009**, *9*, 3289.
[63] A. Perro, G. Lebourdon, S. Henry, S. Lecomte, L. Servant, S. Marre, *React. Chem. Eng.* **2016**, *1*, 577.
[64] X. Yang, Z. Sun, T. Low, H. Hu, X. Guo, F. J. García De Abajo, P. Avouris, Q. Dai, *Adv. Mater.* **2018**, *30*, 1704896.
[65] R. W. Epps, M. S. Bowen, A. A. Volk, K. Abdel-Latif, S. Han, K. G. Reyes, A. Amassian, M. Abolhasani, *Adv. Mater.* **2020**, *32*, 2001626.
[66] B. Pinho, R. L. Hartman, *React. Chem. Eng.* **2017**, *2*, 189.
[67] J. Baek, Y. Shen, I. Lignos, M. G. Bawendi, K. F. Jensen, *Angew. Chem., Int. Ed.* **2018**, *57*, 10915.
[68] Y. Xing, P. S. Dittrich, *Sensors* **2018**, *18*, 134.
[69] R. M. N. Lintag, F. G. D. Leyson, M. S. B. Matibag, K. J. R. Yap, *Mater. Today: Proc.* **2020**, *22*, 185.
[70] S. Marre, A. Adamo, S. Basak, C. Aymonier, K. F. Jensen, *Ind. Eng. Chem. Res.* **2010**, *49*, 11310.
[71] P. Bianchi, G. Petit, J.-C. M. Monbaliu, *React. Chem. Eng.* **2020**, *5*, 1224.
[72] G3 Photo Reactor for Industrial Production, **2018**.
[73] Z. S. Campbell, M. Abolhasani, *React. Chem. Eng.* **2020**, *5*, 1198.
[74] K. Kumar, A. M. Nightingale, S. H. Krishnadasan, N. Kamaly, M. Wylenzinska-Arridge, K. Zeissler, W. R. Branford, E. Ware, A. J. Demello, J. C. Demello, *J. Mater. Chem.* **2012**, *22*, 4704.
[75] R. W. Epps, A. A. Volk, K. Abdel-Latif, M. Abolhasani, *React. Chem. Eng.* **2020**, *5*, 1212.
[76] C. Li, B. Ding, L. Zhang, K. Song, S. Tao, *J. Mater. Chem. C* **2019**, *7*, 9167.
[77] X. Chen, D. Mo, M. Gong, *Micromachines* **2020**, *11*, 1.
[78] P. K. Yuen, *Lab Chip* **2016**, *16*, 3700.
[79] X. Lai, Z. Shi, Z. Pu, P. Zhang, X. Zhang, H. Yu, D. Li, *Microsyst. Nanoeng.* **2020**, *6*, 27.
[80] S. Berciaud, L. Cognet, P. Tamarat, B. Lounis, *Nano Lett.* **2005**, *5*, 515.
[81] J. Wang, W. M. Lau, Q. Li, *J. Appl. Phys.* **2005**, *97*, 114303.
[82] X. Yang, H.-L. Zhou, C.-T. He, Z.-W. Mo, J.-W. Ye, X.-M. Chen, J.-P. Zhang, *Research* **2019**, *2019*, 1.
[83] A. Y. Stakheev, D. A. Bokarev, I. P. Prosvirin, V. I. Bukhtiyarov, *Advanced Nanomaterials for Catalysis and Energy: Synthesis, Characterization and Applications*, Elsevier, Amsterdam **2018**, pp. 295–320.
[84] J. Maes, L. Balcaen, E. Drijvers, Q. Zhao, J. De Roo, A. Vantomme, F. Vanhaecke, P. Geiregat, Z. Hens, *J. Phys. Chem. Lett.* **2018**, *9*, 3093.
[85] J. De Roo, M. Ibáñez, P. Geiregat, G. Nedelcu, W. Walravens, J. Maes, J. C. Martins, I. Van Driessche, M. V. Kovalenko, Z. Hens, *ACS Nano* **2016**, *10*, 2071.
[86] N. S. Marinkovic, K. Sasaki, R. R. Adzic, *J. Electrochem. Soc.* **2018**, *165*, J3222.
[87] R. M. Maceiczyk, D. Hess, F. W. Y. Chiu, S. Stavrakis, A. J. DeMello, *Lab Chip* **2017**, *17*, 3654.
[88] H. Gu, M. H. G. Duits, F. Mugele, *Int. J. Mol. Sci.* **2011**, *12*, 2572.
[89] Y. Liu, G. Chen, J. Yue, *J. Flow Chem.* **2020**, *10*, 103.
[90] A. M. Nightingale, T. W. Phillips, J. H. Bannock, J. C. De Mello, *Nat. Commun.* **2014**, *5*, 3777.
[91] H. M. Xia, S. Y. M. Wan, C. Shu, Y. T. Chew, *Lab Chip* **2005**, *5*, 748.
[92] E. Ringe, M. R. Langille, K. Sohn, J. Zhang, J. Huang, C. A. Mirkin, R. P. Van Duyne, L. D. Marks, *J. Phys. Chem. Lett.* **2012**, *3*, 1479.
[93] S. Cao, F. F. Tao, Y. Tang, Y. Li, J. Yu, *Chem. Soc. Rev.* **2016**, *45*, 4747.

[94] A. R. Poerwoprajitno, L. Gloag, S. Cheong, J. J. Gooding, R. D. Tilley, *Nanoscale* **2019**, *11*, 18995.
[95] G. A. Somorjai, *Surf. Sci.* **1994**, *299*, 849.
[96] M. Chen, B. Wu, J. Yang, N. Zheng, *Adv. Mater.* **2012**, *24*, 862.
[97] J. Baek, P. M. Allen, M. G. Bawendi, K. F. Jensen, *Angew. Chem., Int. Ed.* **2011**, *50*, 627.
[98] P. M. Allen, B. J. Walker, M. G. Bawendi, *Angew. Chem., Int. Ed.* **2010**, *49*, 760.
[99] I. Nakonechnyi, M. Sluydts, Y. Justo, J. Jasieniak, Z. Hens, *Chem. Mater.* **2017**, *29*, 4719.
[100] B. Pinho, L. Torrente-Murciano, *React. Chem. Eng.* **2020**, *5*, 342.
[101] S. Wu, Z. Xin, S. Zhao, S. Sun, *Nano Res.* **2019**, *12*, 2736.
[102] A. A. Kulkarni, V. S. Cabeza, *Langmuir* **2017**, *33*, 14315.
[103] L. Zhang, Y. Wang, L. Tong, Y. Xia, *Nano Lett.* **2014**, *14*, 4189.
[104] G. Niu, L. Zhang, A. Ruditskiy, L. Wang, Y. Xia, *Nano Lett.* **2018**, *18*, 3879.
[105] I. Lignos, L. Protesescu, D. B. Emiroglu, R. MacEiczyk, S. Schneider, M. V. Kovalenko, A. J. DeMello, *Nano Lett.* **2018**, *18*, 1246.
[106] S. Duraiswamy, S. A. Khan, *Part. Part. Syst. Charact.* **2014**, *31*, 429.
[107] A. Yashina, I. Lignos, S. Stavrakis, J. Choo, A. J. Demello, *J. Mater. Chem. C* **2016**, *4*, 6401.
[108] M. Faustini, J. Kim, G. Y. Jeong, J. Y. Kim, H. R. Moon, W. S. Ahn, D. P. Kim, *J. Am. Chem. Soc.* **2013**, *135*, 14619.
[109] J. Wu, L. Qi, H. You, A. Gross, J. Li, H. Yang, *J. Am. Chem. Soc.* **2012**, *134*, 11880.
[110] W. Zhou, J. Wu, H. Yang, *Nano Lett.* **2013**, *13*, 2870.
[111] J. Wu, A. Gross, H. Yang, *Nano Lett.* **2011**, *11*, 798.
[112] G. Niu, M. Zhou, X. Yang, J. Park, N. Lu, J. Wang, M. J. Kim, L. Wang, Y. Xia, *Nano Lett.* **2016**, *16*, 3850.
[113] A. Larrea, V. Sebastian, A. Ibarra, M. Arruebo, J. Santamaria, *Chem. Mater.* **2015**, *27*, 4254.
[114] V. Sebastian, C. D. Smith, K. F. Jensen, *Nanoscale* **2016**, *8*, 7534.
[115] L. Panariello, G. Wu, M. O. Besenhard, K. Loizou, L. Storozhuk, N. T. K. Thanh, A. Gavriilidis, *Materials* **2020**, *13*, 1019.
[116] H. Huang, G. B. Hwang, G. Wu, K. Karu, H. Du Toit, H. Wu, J. Callison, I. P. Parkin, A. Gavriilidis, *Chem. Eng. J.* **2020**, *383*, 123176.
[117] S. Cattaneo, S. Althahban, S. J. Freakley, M. Sankar, T. Davies, Q. He, N. Dimitratos, C. J. Kiely, G. J. Hutchings, *Nanoscale* **2019**, *11*, 8247.
[118] L. Sun, W. Luan, Y. J. Shan, *Nanoscale Res. Lett.* **2012**, *7*, 225.
[119] E. M. Chan, M. A. Marcus, S. Fakra, M. Elnaggar, R. A. Mathies, A. P. Alivisatos, *J. Phys. Chem. A* **2007**, *111*, 12210.
[120] M. Wang, N. Felorzabihi, G. Guerin, J. C. Haley, G. D. Sechloes, M. A. Winnik, *Macromolecules* **2007**, *40*, 6377.
[121] G. Grimaldi, M. J. Van Den Brom, I. Du Fossé, R. W. Crisp, N. Kirkwood, S. Gudjonsdottir, J. J. Geuchies, S. Kinge, L. D. A. Siebbeles, A. J. Houtepen, *J. Phys. Chem. C* **2019**, *123*, 29599.
[122] Y. Shen, M. Abolhasani, Y. Chen, L. Xie, L. Yang, C. W. Coley, M. G. Bawendi, K. F. Jensen, *Angew. Chem., Int. Ed.* **2017**, *56*, 16333.
[123] L. Uson, V. Sebastian, M. Arruebo, J. Santamaria, *Chem. Eng. J.* **2016**, *285*, 286.
[124] L. Gomez, V. Sebastian, S. Irusta, A. Ibarra, M. Arruebo, J. Santamaria, *Lab Chip* **2014**, *14*, 325.
[125] E. M. Chan, A. P. Alivisatos, R. A. Mathies, *J. Am. Chem. Soc.* **2005**, *127*, 13854.
[126] C. B. Kerr, R. W. Epps, M. Abolhasani, *Lab Chip* **2019**, *19*, 2107.
[127] A. J. Harvie, J. C. deMello, *Chem. Eng. J.* **2020**, *394*, 124908.
[128] R. M. Maceiczyk, I. G. Lignos, A. J. deMello, *Curr. Opin. Chem. Eng.* **2015**, *8*, 29.
[129] Y. Orimoto, K. Watanabe, K. Yamashita, M. Uehara, H. Nakamura, T. Furuya, H. Maeda, *J. Phys. Chem. C* **2012**, *116*, 17885.
[130] K. Watanabe, Y. Orimoto, K. Nagano, K. Yamashita, M. Uehara, H. Nakamura, T. Furuya, H. Maeda, *Chem. Eng. Sci.* **2012**, *75*, 292.
[131] Yarpiz, CMA-ES in MATLAB, https://yarpiz.com/235/ypea108-cma-es (accessed: July 2020).
[132] A. Neumaier, SNOBFIT, https://www.mat.univie.ac.at/~neum/software/snobfit/ (accessed: July 2020).
[133] W. Huyer, A. Neumaier, *ACM Trans. Math. Software* **2008**, *35*.
[134] S. Krishnadasan, R. J. C. Brown, A. J. deMello, J. C. deMello, *Lab Chip* **2007**, *7*, 1434.
[135] J. Li, J. Li, R. Liu, Y. Tu, Y. Li, J. Cheng, T. He, X. Zhu, *Nat. Commun.* **2020**, *11*, 2046.
[136] D. M. Olsson, L. S. Nelson, *Technometrics* **1975**, *17*, 45.
[137] L. Wang, L. R. Karadaghi, R. L. Brutchey, N. Malmstadt, *Chem. Commun.* **2020**, *56*, 3745.
[138] C. Igel, N. Hansen, S. Roth, *Evol. Comput.* **2007**, *15*, 1.
[139] R. M. Maceiczyk, A. J. deMello, *J. Phys. Chem. C* **2014**, *118*, 20026.
[140] L. Bezinge, R. M. Maceiczyk, I. Lignos, M. V. Kovalenko, A. J. Demello, *ACS Appl. Mater. Interfaces* **2018**, *10*, 18869.
[141] Y. Yang, F. Wang, Q. Yang, Y. Hu, H. Yan, Y. Z. Chen, H. Liu, G. Zhang, J. Lu, H. L. Jiang, H. Xu, *ACS Appl. Mater. Interfaces* **2014**, *6*, 18163.
[142] H. Guo, B. You, S. Zhao, Y. Wang, G. Sun, Y. Bai, L. Shi, *RSC Adv.* **2018**, *8*, 24002.
[143] A. Antanovich, A. W. Achtstein, A. Matsukovich, A. Prudnikau, P. Bhaskar, V. Gurin, M. Molinari, M. Artemyev, *Nanoscale* **2017**, *9*, 18042.

Amanda A. Volk received her B.S. degree in chemical engineering from the University of Alabama in 2016 and her M.S. degree in chemical engineering from NC State University in 2018. She is currently a Ph.D. candidate in the Department of Chemical and Biomolecular Engineering at NC State. Her work has focused on the advanced manufacturing of semiconductor materials using vapor and solution-phase molecular and atomic-layer deposition. Her research interests include the continuous manufacturing of colloidal nanomaterials and the fabrication of next-generation semiconductor-based technologies.

Robert W. Epps is currently a Doctoral Candidate at North Carolina State University. He received his B.E. in Chemical Engineering at Vanderbilt University (2016) and his M.S. in Chemical Engineering at North Carolina State University (2018). He currently works in developing high-throughput and autonomous flow chemistry screening strategies towards the production of next-generation colloidal nanomaterials. His research interests include system automation, machine learning guided experimentation, and self-optimizing reactors.

Milad Abolhasani is an Assistant Professor in the Department of Chemical and Biomolecular Engineering at North Carolina State University. He received his Ph.D. degree (2014) from the Department of Mechanical and Industrial Engineering in collaboration with the Department of Chemistry at the University of Toronto. Prior to joining NC State University in 2016, he was an NSERC postdoctoral fellow in the Department of Chemical Engineering at Massachusetts Institute of Technology. Dr. Abolhasani leads a diverse research group that studies flow chemistry strategies tailored towards accelerated development and manufacturing of advanced materials using autonomous robotic experimentation in flow.